

Supplementary information

**From a Simple *Push-Pull* Dye to a Functional Material by Assembly with CuBr**

Léo Boivin,<sup>1</sup> Élodie V. d'Astous,<sup>1</sup> Adrien Schlachter,<sup>2</sup> Daniel Fortin,<sup>1</sup> Paul-Ludovic Karsenti,<sup>1</sup> Christophe Lescop,<sup>2</sup> Philippe Dauphin Ducharme,<sup>1</sup> Pierre D. Harvey<sup>1\*</sup>

<sup>1</sup>*Département de Chimie, Université de Sherbrooke QC J1K 2R1 Canada*

<sup>2</sup>*ISCR (Institut des Sciences Chimiques de Rennes) UMR 6226, CNRS, INSA Rennes, University Rennes, F-35000 Rennes, France*

## TABLE OF CONTENTS

Figure S1. FTIR and FT-Raman spectra of <b>L</b> and <b>UDS-6</b> .	3
Figure S2. Absorbance spectrum of <b>UDS-6</b> compared to that of MgSO <sub>4</sub> prepared under similar conditions.	4
Table S1. Crystal data, data collection, and structure refinement parameters for <b>L</b> and <b>UDS-6</b> .	5
Figure S3. Left : Steady-state spectra of <b>L</b> in a 2-MeTHF solution at 293 K.	6
Figure S4. Photoluminescence decay and lifetime of <b>L</b> in a 2-MeTHF solution monitored at 293 K and 700 nm (LE, aggregate band).	7
Figure S5. Steady-state spectra of <b>L</b> in a 2-MeTHF solution at 77 K.	8
Figure S6. Photoluminescence decay and lifetime of <b>L</b> in a 2-MeTHF solution monitored at 293 K and 450 nm (HE, monomer band).	9
Figure S7. Frontier molecular orbitals of a single <b>L</b> molecule.	10
Figure S8. Frontier molecular orbitals of a tetrameric solid-state arrangement of <b>L</b> molecules.	10
Figure S9. Photoluminescence decay and lifetime of <b>L</b> in a 2-MeTHF solution monitored at 77 K.	11
Figure S10. Photoluminescence decay and shorter lifetimes of <b>L</b> in the solid state at 293 K	12
Figure S11. Photoluminescence decay and longer lifetimes of <b>L</b> in the solid state at 293 K.	13
Figure S12. Photoluminescence decay and lifetimes of <b>L</b> in the solid state at 77 K.	14
Figure S13. Full PXRD pattern of <b>UDS-6</b>	15
Figure S14. Steady-state spectra of <b>UDS-6</b> in wavenumber axis.	16
Table S2. List of the first 100 electronic transitions for Cu <sub>2</sub> Br <sub>2</sub> <b>L</b> <sub>4</sub> , with major orbital contributions.	17
Figure S15. Selected molecular orbitals of the Cu <sub>2</sub> Br <sub>2</sub> <b>L</b> <sub>4</sub> cluster.	19
Figure S16. Calculated UV-Vis spectrum (in blue) of <b>UDS-6</b> compared to the experimental spectrum (in red).	20
Figure S17. Photoluminescence decay of <b>UDS-6</b> at room temperature.	21
Figure S18. Photoluminescence decay and lifetime of <b>UDS-6</b> at 77K.	22
Figure S19. Photoluminescence spectra of different powders. There is no significant interaction between <b>UDS-6</b> and <b>PC71bm</b> , as the luminescence of <b>PC71bm</b> is not reduced by at least half of the initial intensity.	23
Figure S20. Photoluminescence quenching of ZnTPP by <b>UDS-6</b> seen by the decrease in the PL of both chromophores.	24
Figure S21. Photoluminescence decay and lifetimes of ZnTPP in the solid state.	25
Figure S22. Photoluminescence decay and lifetimes of ZnTPP in a solid state blend with <b>UDS-6</b> .	26
Figure S23. Photoluminescence decay and lifetimes of <b>UDS-6</b> in a blend with ZnTPP.	27
Figure S24. Cyclic voltammetry plot of <b>L</b> in dry degassed ACN.	28
Figure S25. Cyclic voltammetry plot of <b>L</b> in dry degassed DCM.	29
Figure S26. Cyclic voltammetry plot of <b>L</b> in dry degassed THF. Since <b>L</b> precipitates on the electrode after the first cycle, only this first cycle is presented here.	30
Figure S27. Kinetic parameter determination for <b>L</b> using rotating disk electrodes adapted for a quasi-reversible system.	31
Figure S28. Cyclic voltammetry of a spin-coated dispersed film of <b>UDS-6</b> shows no difference between dark conditions (left) and simulated solar irradiance exposure (right).	32
Figure S29. Thermogravimetric analysis plot of the thermal degradation of <b>UDS-6</b> .	33
Figure S30. Powder X-ray diffractogram of a pristine sample of <b>UDS-6</b> , and a sample of <b>UDS-6</b> soaked for one hour in aqueous 0.5M Na <sub>2</sub> SO <sub>4</sub> .	34

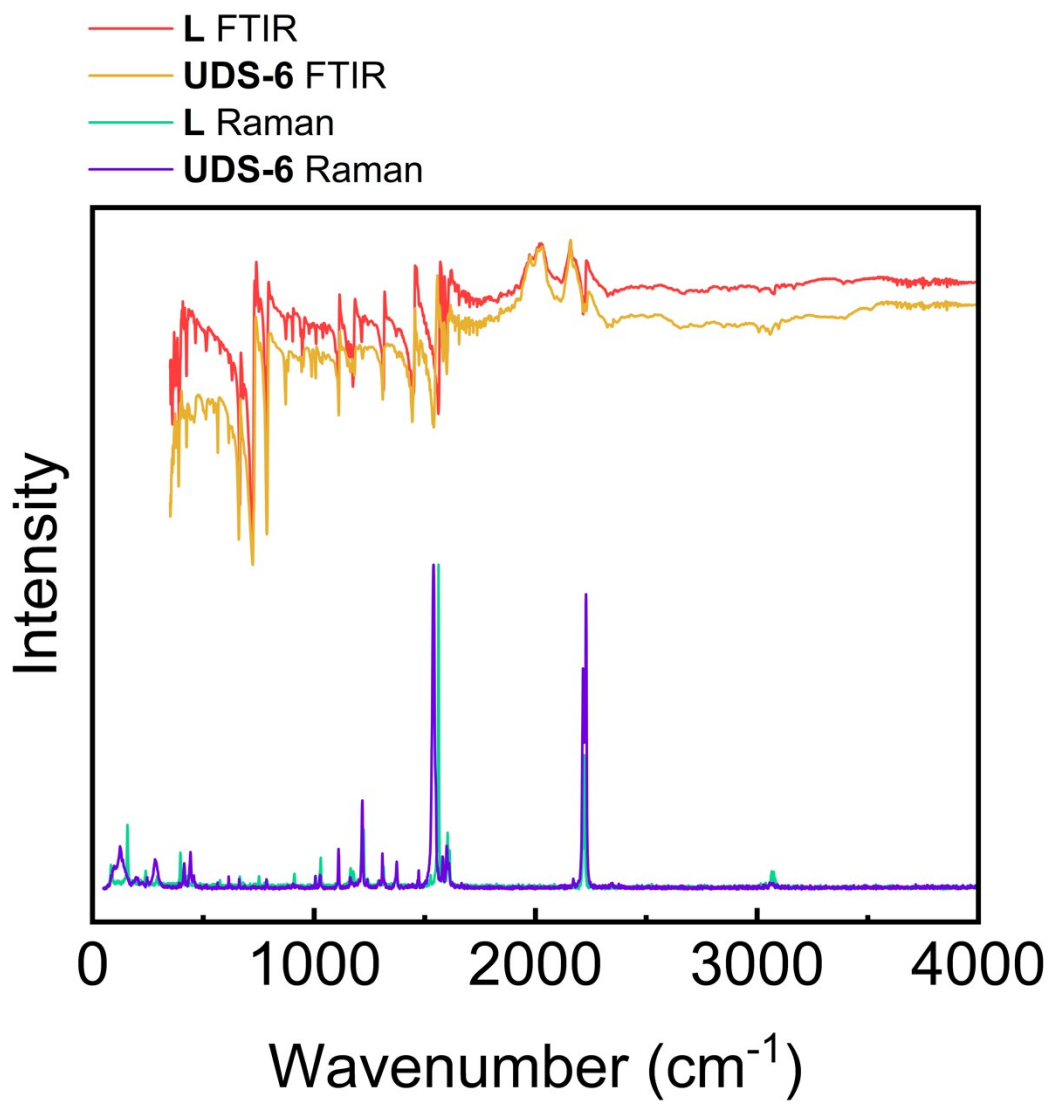


Figure S1. FTIR and FT-Raman spectra of **L** and **UDS-6**.

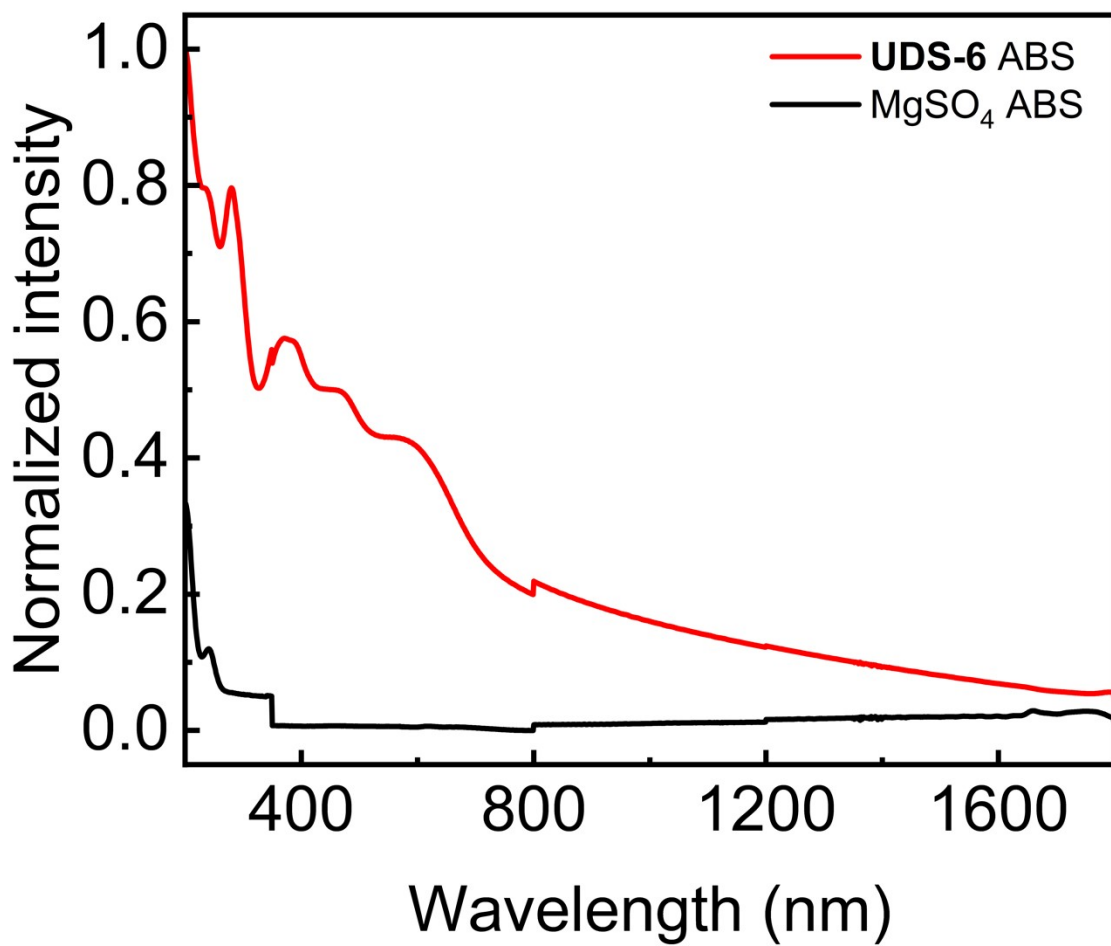


Figure S2. Absorbance spectrum of **UDS-6** compared to that of MgSO<sub>4</sub> prepared under similar conditions. This shows that there is minimal impact from diffusion phenomena of light onto the powder particles in transmission mode.

Table S1. Crystal data, data collection, and structure refinement parameters for **L** and **UDS-6**.

Compound	<b>L</b>	<b>UDS-6</b>
Formula	C <sub>16</sub> H <sub>8</sub> N <sub>2</sub>	C <sub>16</sub> H <sub>8</sub> BrCuN <sub>2</sub>
Formula weight /g.mol <sup>-1</sup>	228.24	743.41
Temperature /K	173(2)	173.21
Crystal system	Orthorhombic	Monoclinic
Space group	P2 <sub>1</sub> 2 <sub>1</sub> 2 <sub>1</sub>	P2 <sub>1</sub> /n
a /Å	3.8662(5)	13.4481(17)
b /Å	9.2585(12)	14.4239(18)
c /Å	30.669(4)	14.2542(18)
α /°	90	90
β /°	90	113.978(2)
γ /°	90	90
Volume /Å <sup>3</sup>	1097.8(2)	2526.3(6)
Z	4	4
ρ <sub>calc</sub> /gcm <sup>-3</sup>	1.381	1.9544
μ /mm <sup>-1</sup>	0.083	4.879
F(000)	472	1457.0
Crystal size /mm <sup>3</sup>	0.210 × 0.210 × 0.700	0.26 × 0.085 × 0.075
Radiation	Mo Kα (λ = 0.71073)	Mo Kα (λ = 0.71073)
2θ range for data collection /°	2.30 to 25.88 -4 ≤ h ≤ 3 -11 ≤ k ≤ 11 -36 ≤ l ≤ 37	3.52 to 52.78 -16 ≤ h ≤ 15 -15 ≤ k ≤ 18 -17 ≤ l ≤ 17
Index ranges		
Reflections collected	5706	33196
Independent reflections	1993 [R <sub>int</sub> = 0.0374}]	5155 [R <sub>int</sub> = 0.0984, R <sub>sigma</sub> = 0.0845]
Data/restraints/parameters	1993/0/163	5155/0/361
Goodness-of-fit on F <sup>2</sup>	1.129	1.088
Final R indexes [I ≥ 2σ (I)]	R <sub>1</sub> = 0.0484, wR <sub>2</sub> = 0.1122	R <sub>1</sub> = 0.0530, wR <sub>2</sub> = 0.1001
Final R indexes [all data]	R <sub>1</sub> = 0.0531, wR <sub>2</sub> = 0.1141	R <sub>1</sub> = 0.1118, wR <sub>2</sub> = 0.1219
Largest diff. peak/hole /eÅ <sup>-3</sup>	0.205/-0.268	1.84/-1.69

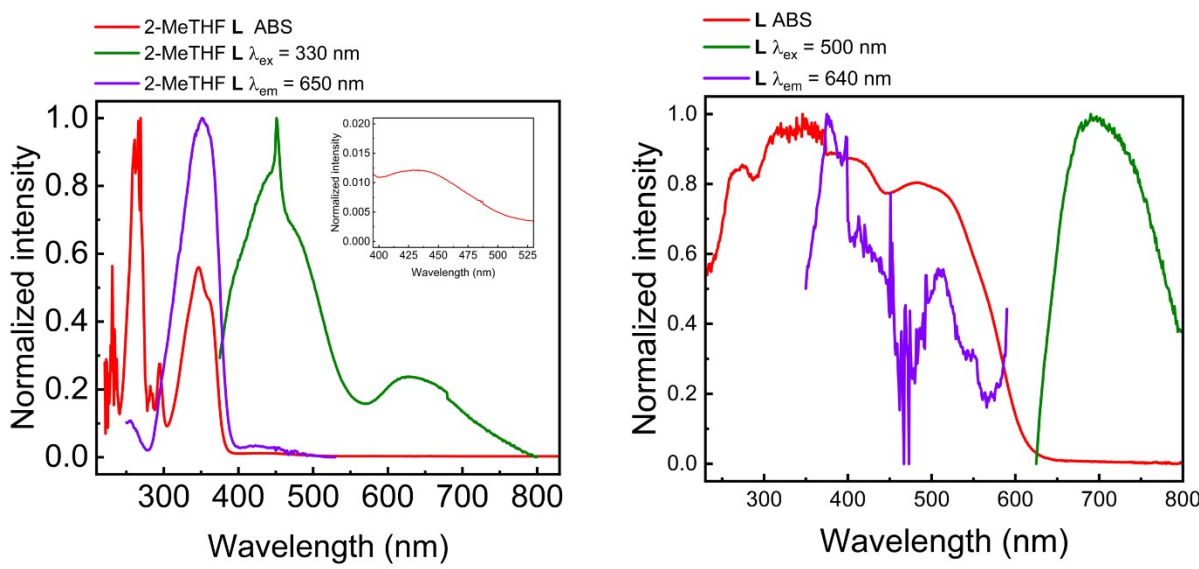


Figure S3. Left : Steady-state spectra of **L** in a 2-MeTHF solution at 293 K. The artefact near 450 nm in the emission spectrum is an artefact due to the machine that could not be removed. The inset shows the forbidden absorbance band near 430 nm. Right : steady-state spectra of **L** in the solid state at 293 K.

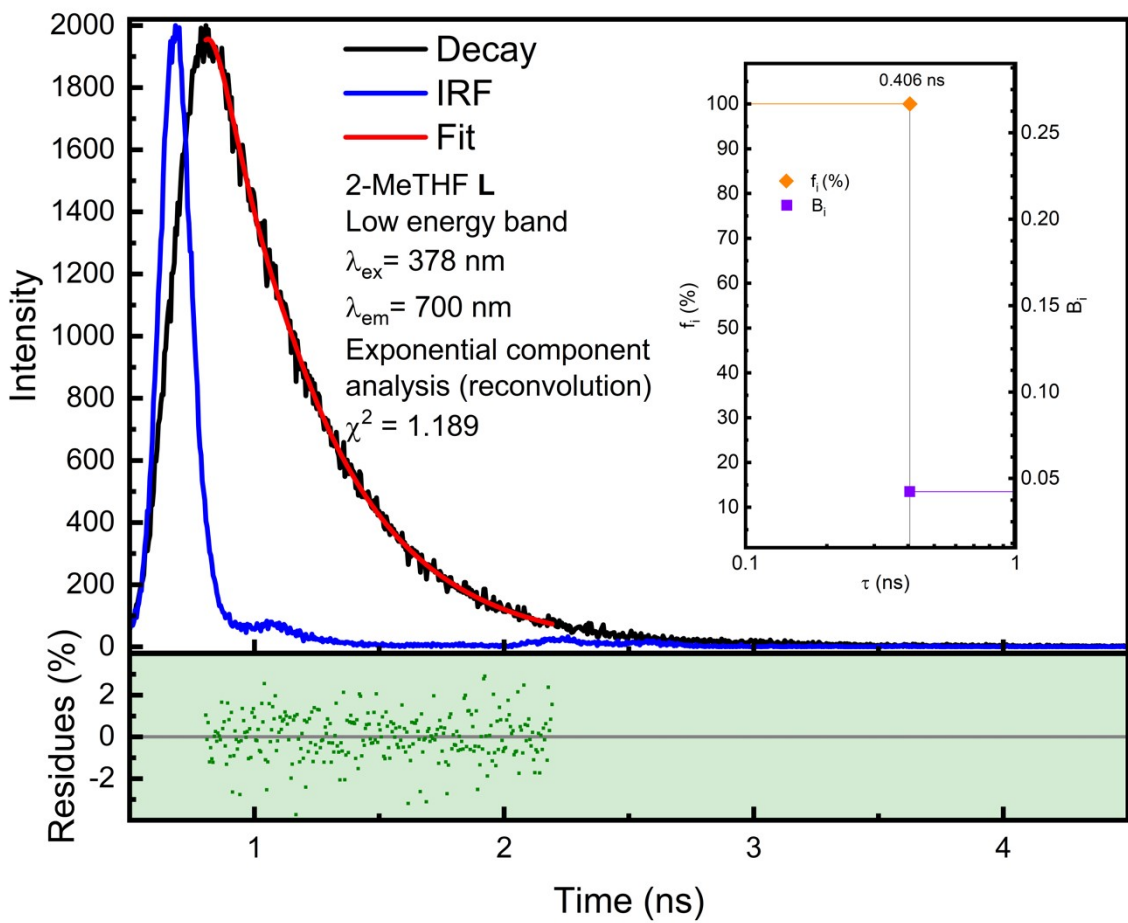


Figure S4. Photoluminescence decay and lifetime of **L** in a 2-MeTHF solution monitored at 293 K and 700 nm (LE, aggregate band).

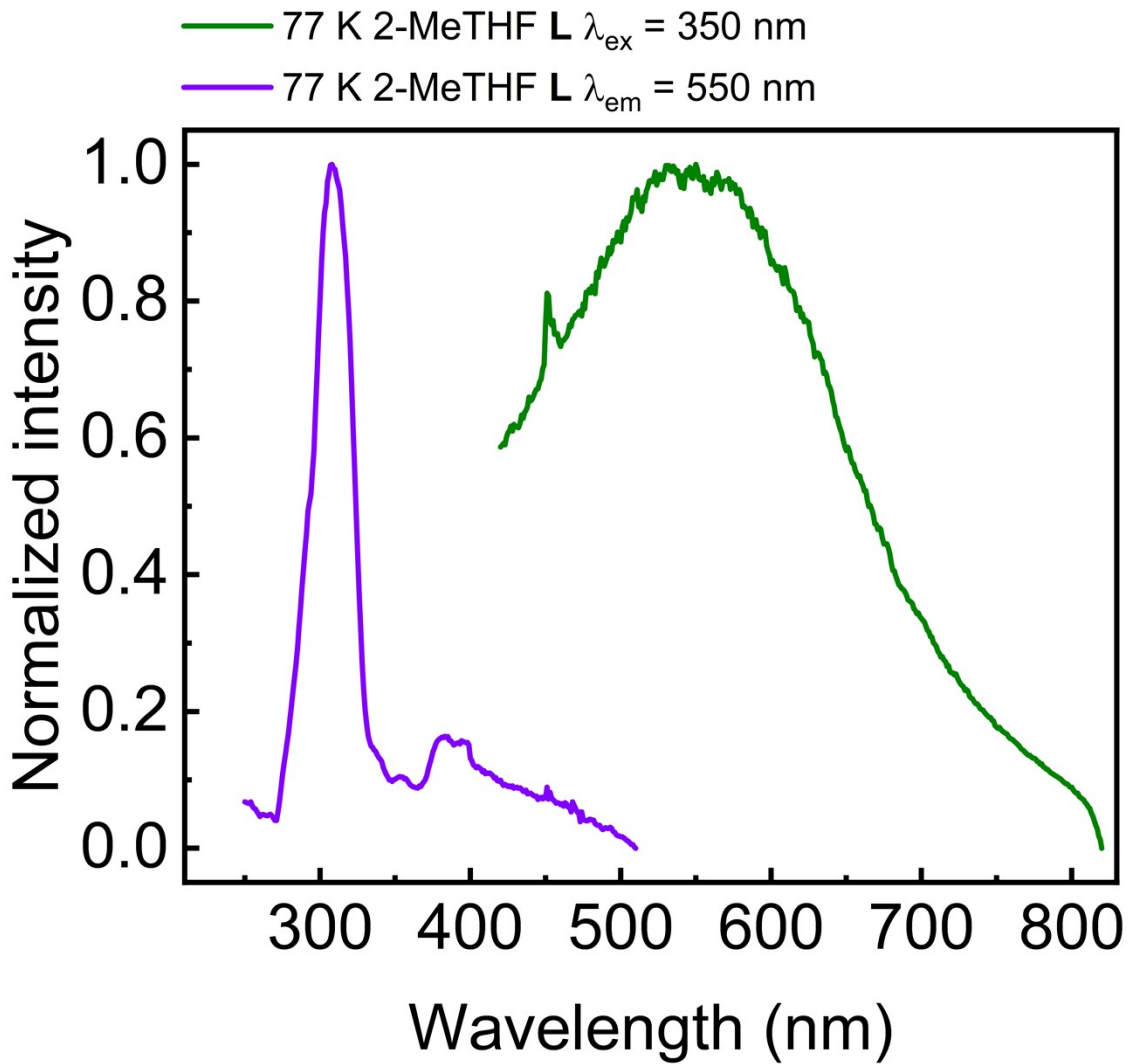


Figure S5. Steady-state spectra of **L** in a 2-MeTHF solution at 77 K.

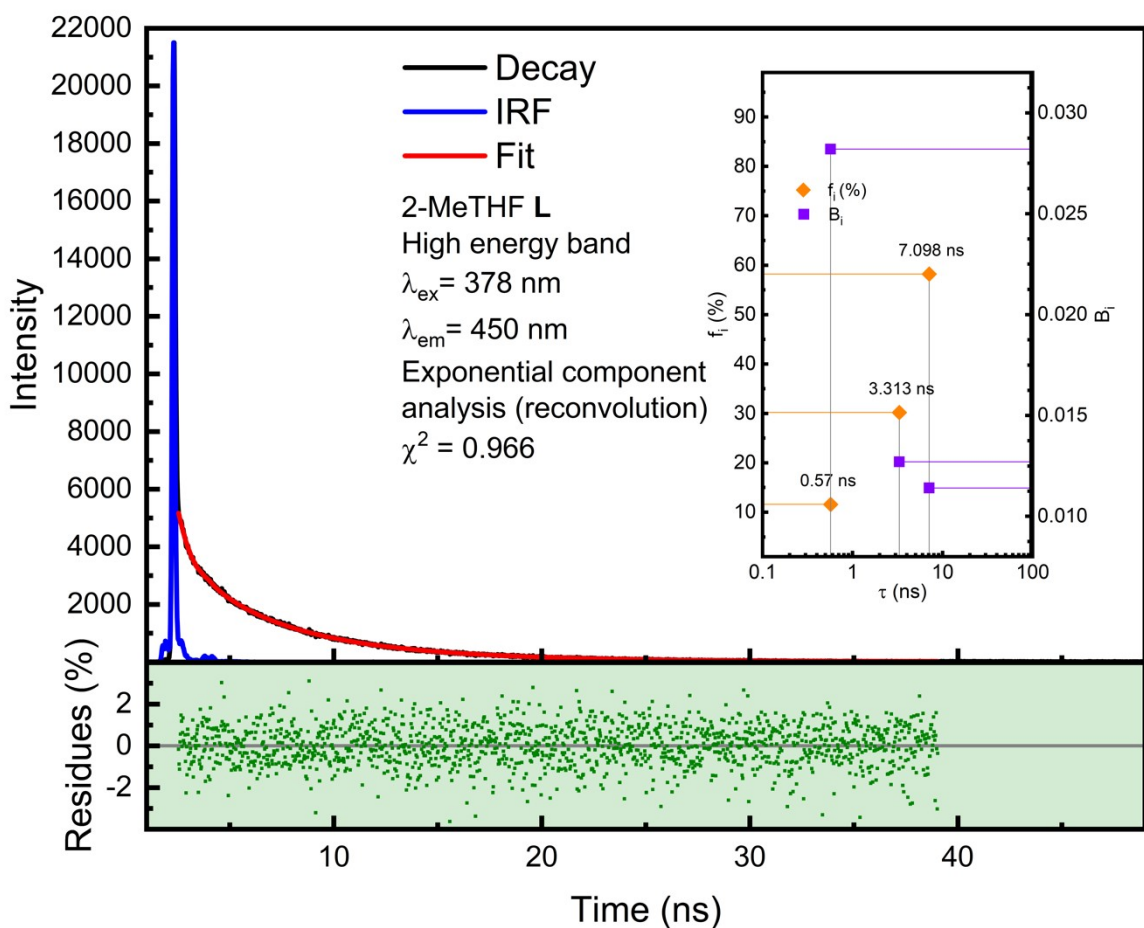


Figure S6. Photoluminescence decay and lifetime of **L** in a 2-MeTHF solution monitored at 293 K and 450 nm (HE, monomer band).

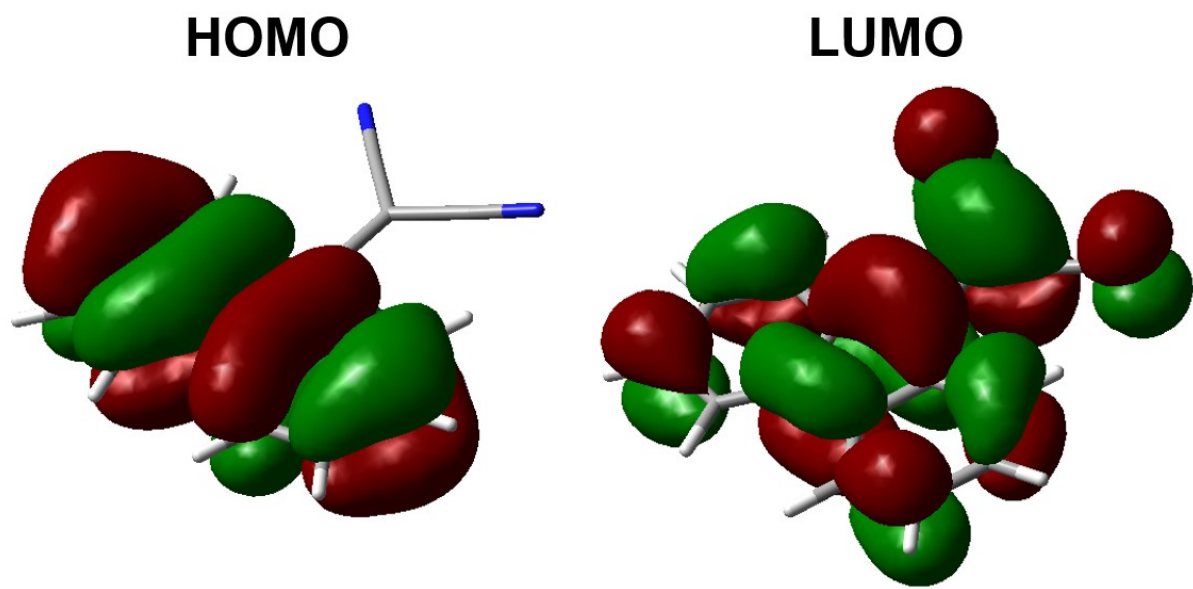


Figure S7. Frontier molecular orbitals of a single **L** molecule.

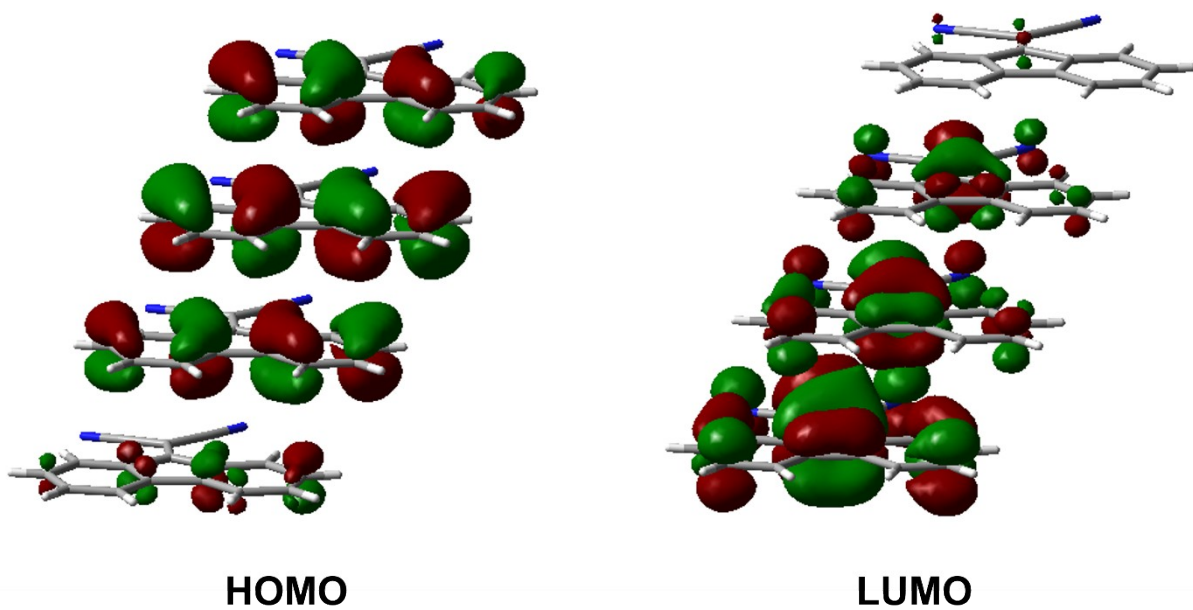


Figure S8. Frontier molecular orbitals of a tetrameric solid-state arrangement of **L** molecules.

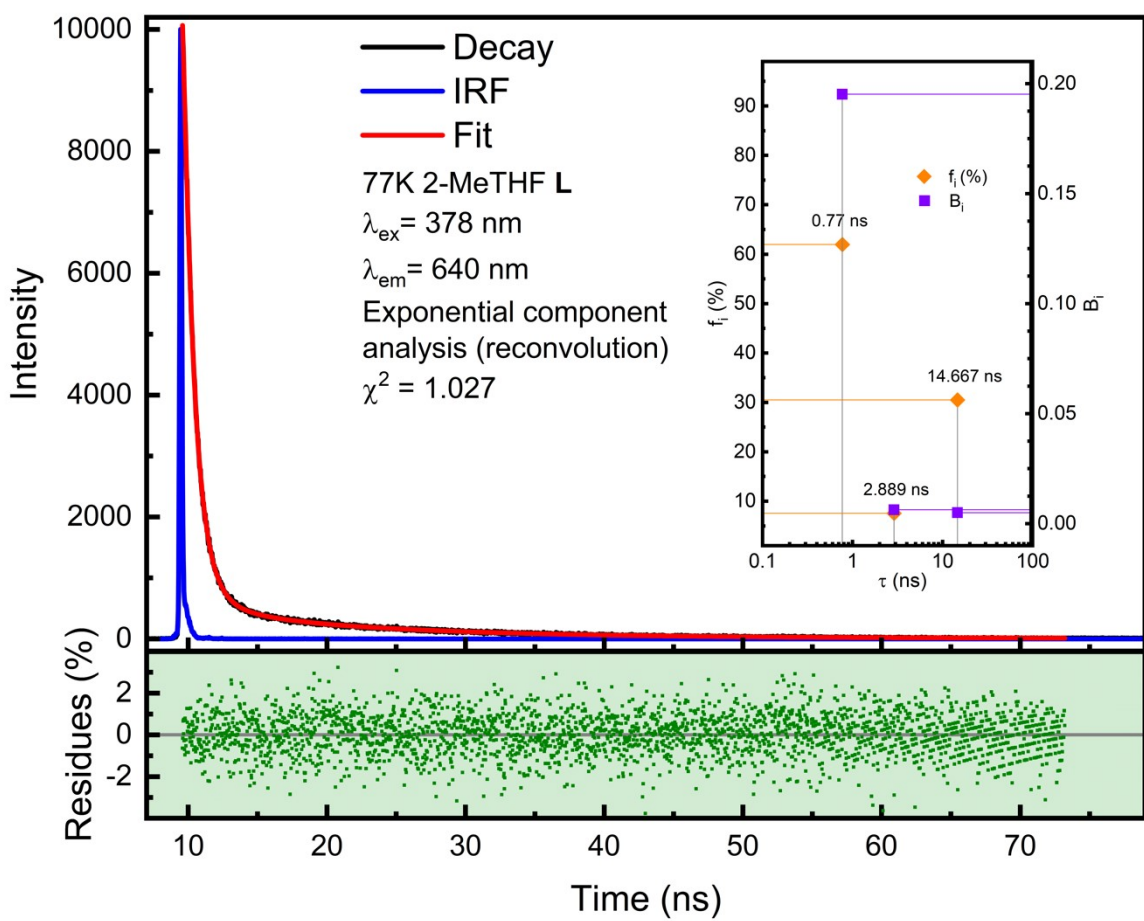


Figure S9. Photoluminescence decay and lifetime of **L** in a 2-MeTHF solution monitored at 77 K.

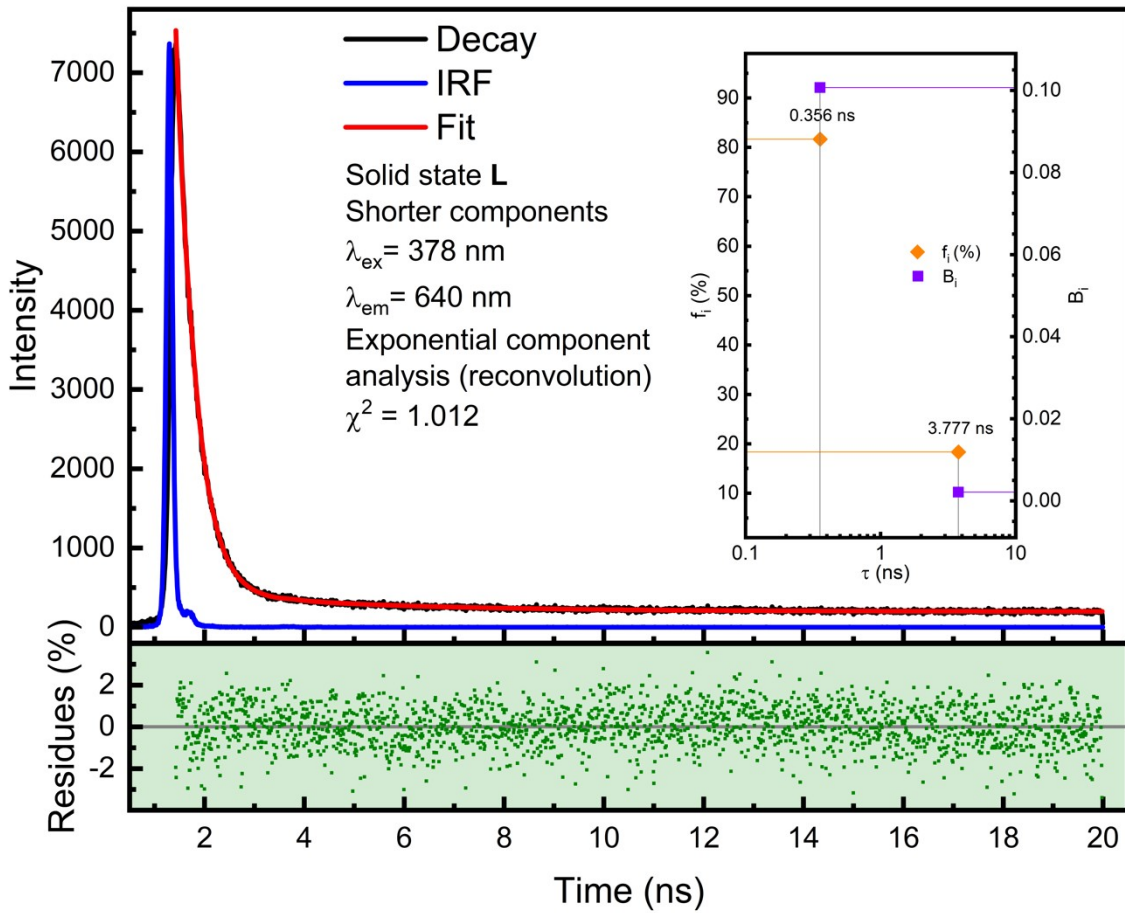


Figure S10. Photoluminescence decay and shorter lifetimes of **L** in the solid state at 293 K.

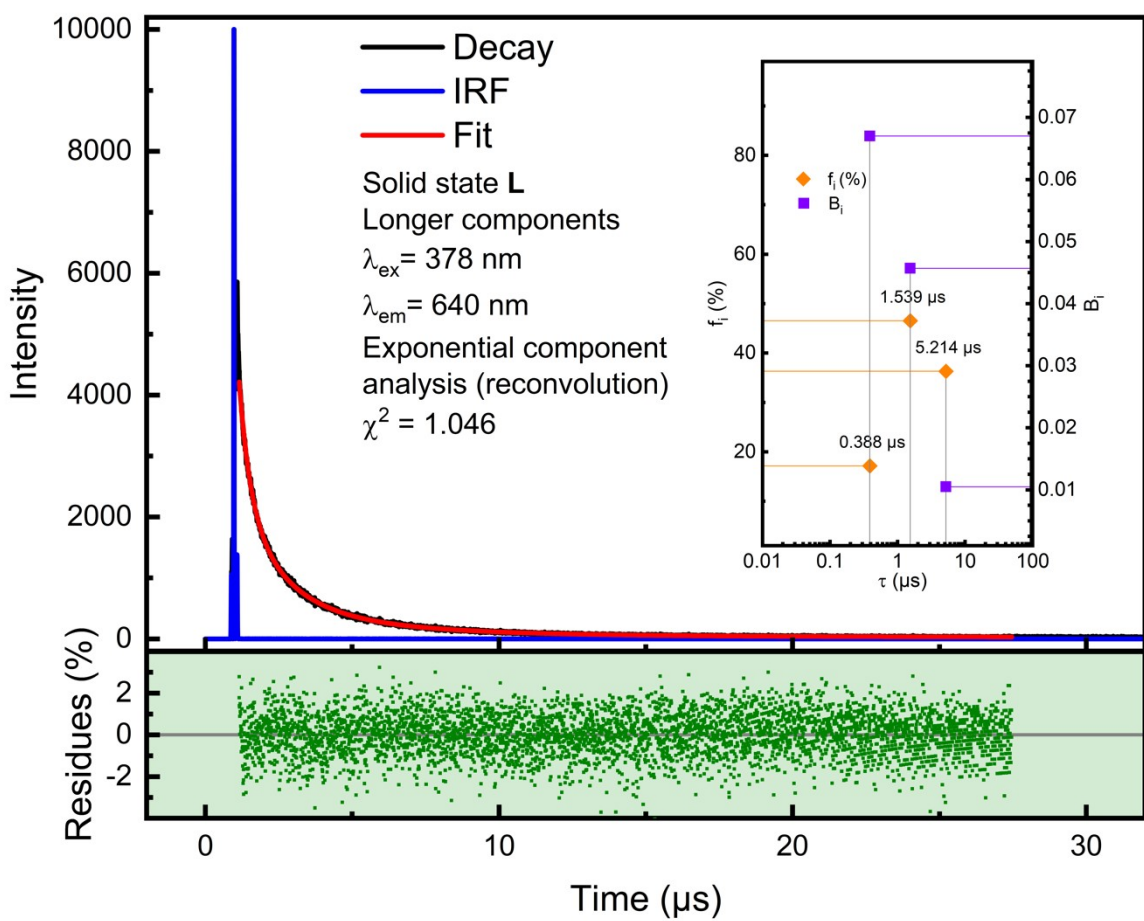


Figure S11. Photoluminescence decay and longer lifetimes of **L** in the solid state at 293 K.

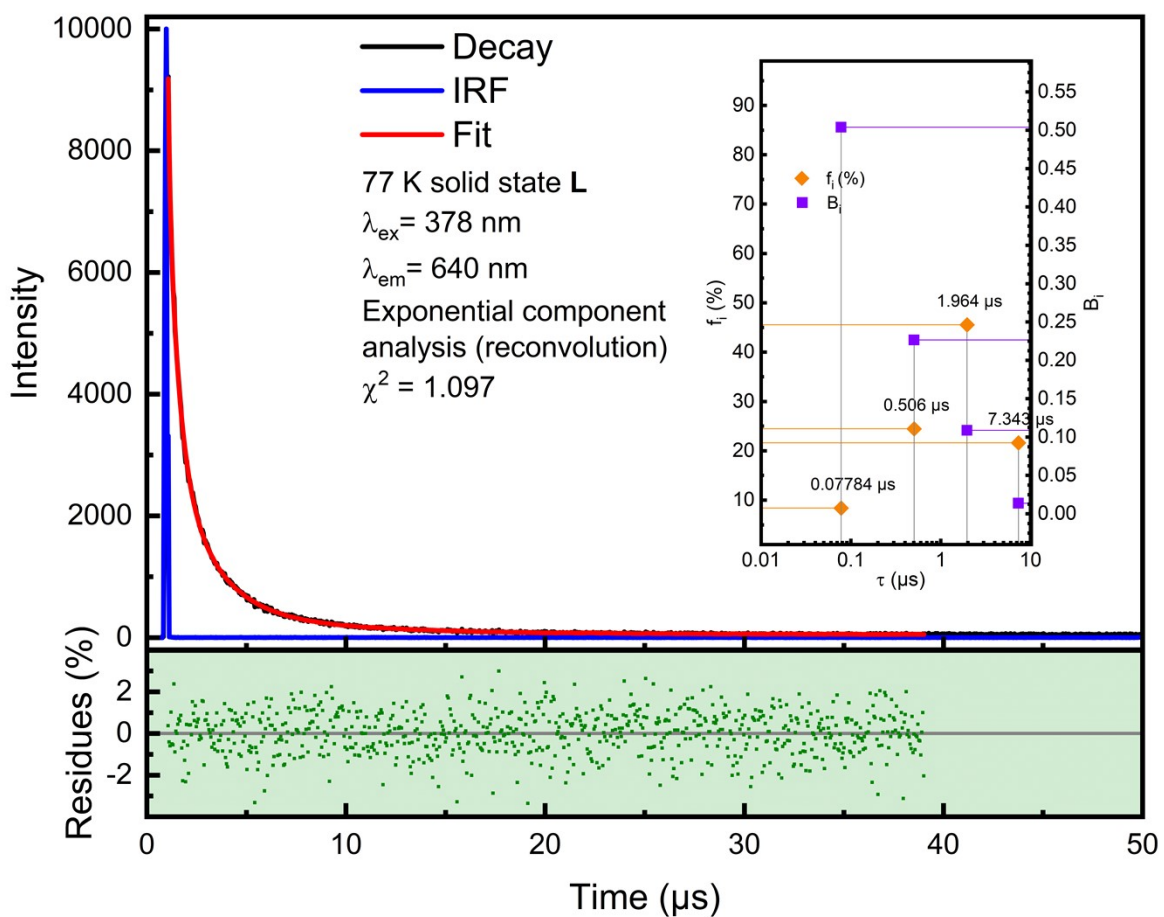


Figure S12. Photoluminescence decay and lifetimes of L in the solid state at 77 K.

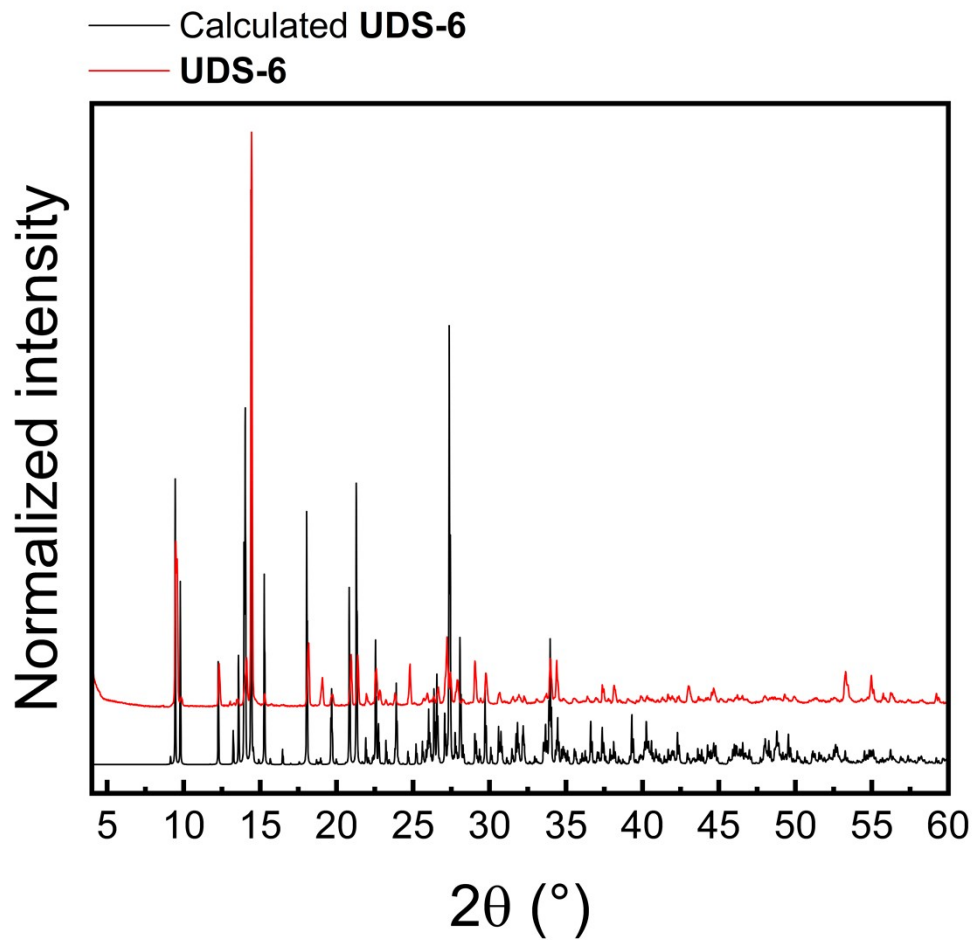


Figure S13. Full PXRD pattern of **UDS-6**.

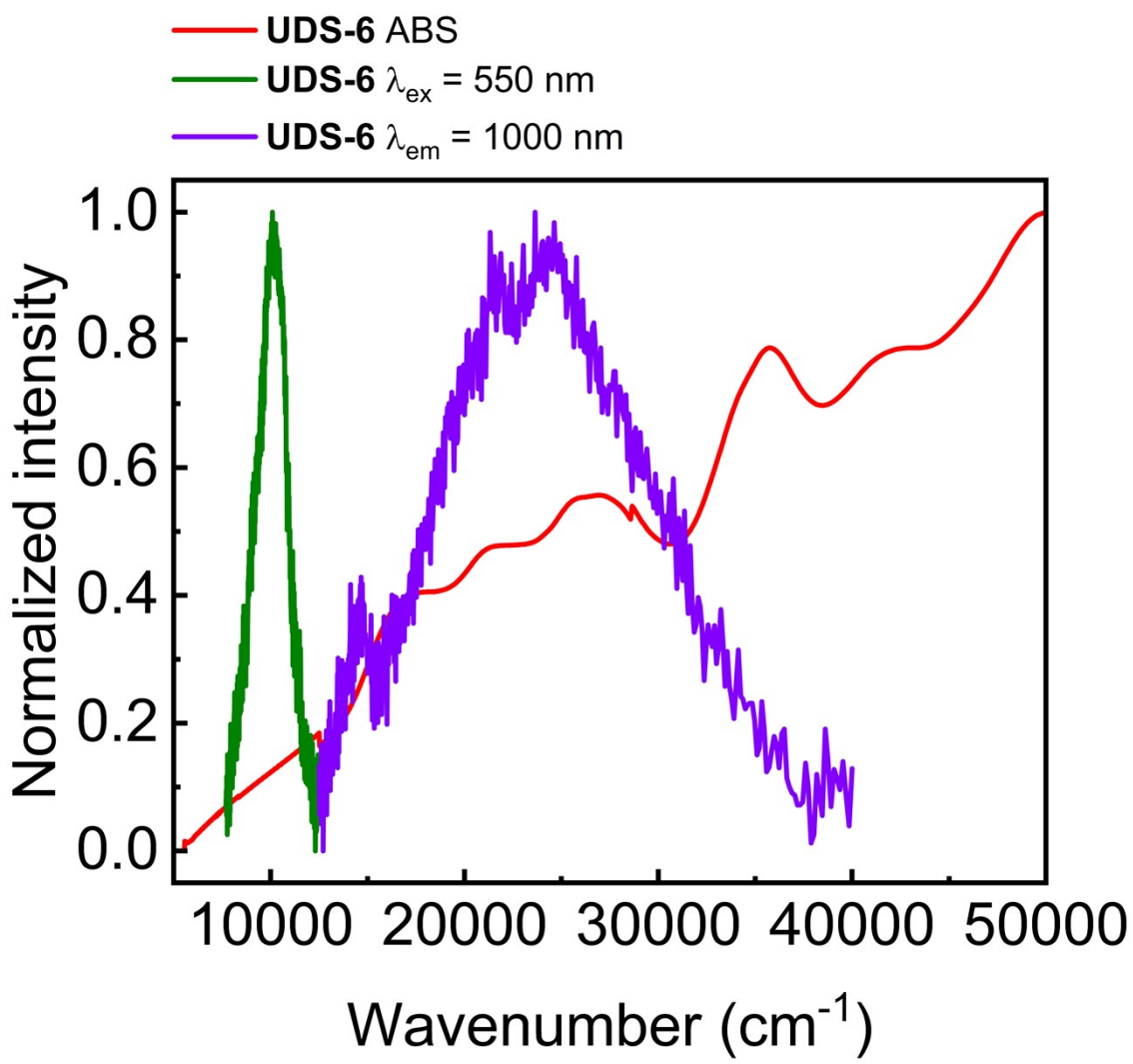


Figure S14. Steady-state spectra of **UDS-6** in wavenumber axis.

Table S2. List of the first 100 electronic transitions for  $\text{Cu}_2\text{Br}_2\mathbf{L}_4$ , with major orbital contributions.

No	$\lambda$ (nm)	Osc. strength	Major contribs
1	1052	0.0237	H-1→LUMO (35%), HOMO→LUMO (48%)
2	1028	0.0068	H-1→LUMO (45%), HOMO→LUMO (25%), HOMO→L+2 (11%)
3	1008	0.0807	H-1→L+2 (10%), HOMO→LUMO (11%), HOMO→L+1 (20%), HOMO→L+2 (44%)
4	988	0.0334	HOMO→L+1 (34%), HOMO→L+2 (25%), HOMO→L+3 (25%)
5	975	0.0202	H-1→L+1 (28%), H-1→L+2 (28%)
6	962	0.0098	H-1→L+1 (13%), H-1→L+2 (25%), HOMO→L+1(11%), HOMO→L+3 (22%)
7	943	0.0073	H-2→LUMO (42%), H-1→L+1 (19%), H-1→L+2(12%)
8	933	0.0038	H-2→LUMO (11%), H-1→L+2 (19%), H-1→L+3 (58%)
9	929	0.0057	H-2→LUMO (10%), H-1→L+1 (20%), H-1→L+2 (14%), HOMO→L+3 (22%)
10	886	0.0069	H-2→L+1 (45%), H-2→L+2 (14%)
11	855	0.0024	H-2→L+1 (24%), H-2→L+2 (57%)
12	845	0.0011	H-2→L+3 (73%)
13	766	0.0087	H-4→LUMO (51%)
14	747	0.0010	H-5→LUMO (34%), H-3→LUMO (39%)
15	740	0.0025	H-4→L+1 (13%), H-5→L+2 (27%), H-4→L+1 (15%), H-3→L+2 (12%)
16	723	0.0058	H-5→L+1 (13%), H-5→L+2 (27%), H-4→L+1 (15%), H-3→L+2 (12%)
17	721	0.0019	H-5→L+2 (19%), H-4→L+1 (23%), H-3→L+1 (11%)
18	720	0.0020	H-3→L+2 (15%), H-3→L+3 (60%)
19	714	0.0574	H-6→LUMO (15%), H-5→LUMO (11%), H-5→L+3 (16%), H-3→LUMO (25%)
20	708	0.0004	H-5→L+1 (27%), H-5→L+2 (11%), H-3→L+1 (33%)
21	702	0.0817	H-4→L+2 (42%), H-3→L+1 (20%)
22	696	0.0254	H-5→L+3 (37%), H-4→L+3 (30%)
23	692	0.0346	H-6→LUMO (46%), H-5→L+3 (10%)
24	672	0.0476	H-6→L+2 (53%)
25	670	0.0042	H-6→L+1 (43%), H-6→L+2 (10%), H-4→L+2 (11%)
26	664	0.0093	H-6→L+3 (49%), H-4→L+3 (23%)
27	626	0.0360	H-6→L+3 (18%), H-5→LUMO (10%), H-5→L+1 (10%), H-4→L+3 (19%)
28	620	0.0074	H-6→L+2 (19%), H-6→L+3 (10%), H-5→L+1 (10%), H-5→L+2 (10%)
29	605	0.0001	H-9→LUMO (12%), H-8→LUMO (21%), H-7→LUMO (41%), H-6→LUMO (14%)
30	590	0.0073	H-8→LUMO (11%), H-8→L+2 (15%), H-7→L+1 (10%), H-7→L+3 (25%)
31	589	0.0011	H-8→L+2 (17%), H-7→L+2 (12%), H-7→L+3 (25%)
32	586	0.0483	H-8→LUMO (10%), H-7→LUMO (14%), H-7→L+1 (35%), H-7→L+2 (16%)
33	574	0.0143	H-8→L+1 (35%), H-8→L+2 (27%)
34	569	0.0073	H-9→L+3 (10%), H-8→L+2 (11%), H-8→L+3 (61%)
35	557	0.0500	H-9→LUMO (13%), H-9→L+3 (10%), H-7→L+2 (20%), H-7→L+3 (25%)
36	549	0.0035	H-9→L+2 (16%), H-7→L+1 (28%), H-7→L+3 (12%)
37	544	0.0048	H-9→LUMO (57%), H-8→LUMO (20%)
38	536	0.1510	H-9→L+2 (44%), H-8→L+1 (11%), H-7→L+2 (15%)
39	532	0.0000	H-9→L+1 (65%), H-9→L+2 (11%), H-8→L+1 (18%)
40	526	0.0045	H-9→L+3 (71%)
41	504	0.0007	H-10→L+2 (90%)
42	491	0.0008	H-12→LUMO (97%)
43	487	0.0003	H-11→L+3 (88%)
44	473	0.0012	H-13→L+1 (96%)
45	451	0.0001	H-10→LUMO (95%)
46	428	0.0002	H-11→L+1 (92%)
47	424	0.0000	H-11→LUMO (95%)
48	423	0.0000	H-10→L+1 (99%)
49	412	0.0001	H-10→L+3 (94%)

50	407	0.0001	H-11→L+2 (93%)
51	405	0.0000	H-13→LUMO (17%), H-13→L+2 (80%)
52	404	0.0000	H-12→L+2 (10%), H-12→L+3 (83%)
53	397	0.0000	H-13→LUMO (83%), H-13→L+2 (17%)
54	397	0.0000	H-12→L+2 (89%)
55	391	0.0000	H-12→L+1 (92%)
56	391	0.0000	H-13→L+3 (94%)
57	383	0.0005	HOMO→L+4 (97%)
58	380	0.0003	HOMO→L+5 (97%)
59	377	0.0016	H-14→LUMO (94%)
60	373	0.0027	HOMO→L+6 (11%), HOMO→L+7 (76%)
61	373	0.0002	HOMO→L+6 (81%), HOMO→L+7 (12%)
62	369	0.0155	H-14→L+1 (66%), H-14→L+2 (24%)
63	366	0.0155	H-14→L+1 (13%), H-14→L+2 (27%)
64	366	0.0089	H-14→L+1 (15%), H-14→L+2 (29%), HOMO→L+8 (32%)
65	365	0.0057	H-1→L+4 (89%)
66	364	0.0335	H-14→L+3 (72%)
67	362	0.0005	H-1→L+5 (97%)
68	362	0.029	H-15→LUMO (92%)
69	358	0.0046	HOMO→L+9 (62%)
70	357	0.0004	H-1→L+6 (29%), H-1→L+7 (52%)
71	356	0.0006	H-1→L+6 (65%), H-1→L+7 (26%)
72	355	0.0007	H-15→L+1 (89%)
73	353	0.1070	H-16→LUMO (55%)
74	352	0.0055	H-16→LUMO (15%), H-2→L+8 (11%), H-1→L+8 (26%)
75	350	0.0227	H-15→L+2 (11%), H-2→L+8 (21%)
76	350	0.0221	H-2→L+4 (80%)
77	347	0.2127	H-16→L+1 (27%), H-15→L+3 (16%)
78	347	0.0149	H-2→L+5 (87%)
79	346	0.0384	H-16→L+1 (24%), HOMO→L+10 (12%)
80	345	0.0027	HOMO→L+10 (10%), HOMO→L+11 (33%)
81	345	0.0096	H-2→L+7 (13%), H-2→L+9 (10%), HOMO→L+11 (18%)
82	344	0.0137	HOMO→L+10 (50%)
83	343	0.0394	H-16→L+1 (12%), H-2→L+6 (13%), H-1→L+8 (28%)
84	342	0.0007	H-16→L+2 (43%), H-16→L+3 (10%), H-15→L+2 (10%), H-15→L+3 (18%)
85	342	0.0009	H-16→L+3 (46%), H-15→L+2 (15%)
86	341	0.0065	H-2→L+6 (73%)
87	340	0.0522	H-23→LUMO (11%), H-17→LUMO (23%), H-17→L+2 (13%), H-2→L+7 (20%)
88	339	0.0576	H-17→L+2 (37%), H-2VL+7 (11%), H-1→L+9 (20%)
89	338	0.0031	H-23→LUMO (25%), H-17→L+2 (20%), H-1→L+9 (21%)
90	337	0.0207	H-17→L+3 (11%), H-2→L+7 (26%), H-2→L+9 (14%), H-1→L+9 (15%)
91	336	0.0361	H-17→L+3 (54%)
92	335	0.1214	H-19→L+2 (19%), H-18→L+2 (31%)
93	335	0.0727	H-22→L+1 (36%), H-17→L+1 (17%)
94	334	0.1371	H-23→LUMO (16%), H-22→L+1 (11%), H-17→LUMO (20%), H-17→L+3 (14%)
95	332	0.0005	H-21→LUMO (10%), H-18→LUMO (28%), H-17→LUMO (12%)
96	331	0.0433	H-21→LUMO (45%), H-19→LUMO (11%)
97	331	0.1329	H-18→L+2 (20%), H-3→L+4 (16%), H-1→L+11 (18%)
98	330	0.0587	H-3→L+4 (71%)
99	329	0.0366	H-18→L+1 (21%), H-18→L+3 (18%), H-17→L+1 (24%)
100	329	0.0300	H-18→L+3 (55%), H-17→L+1 (14%)

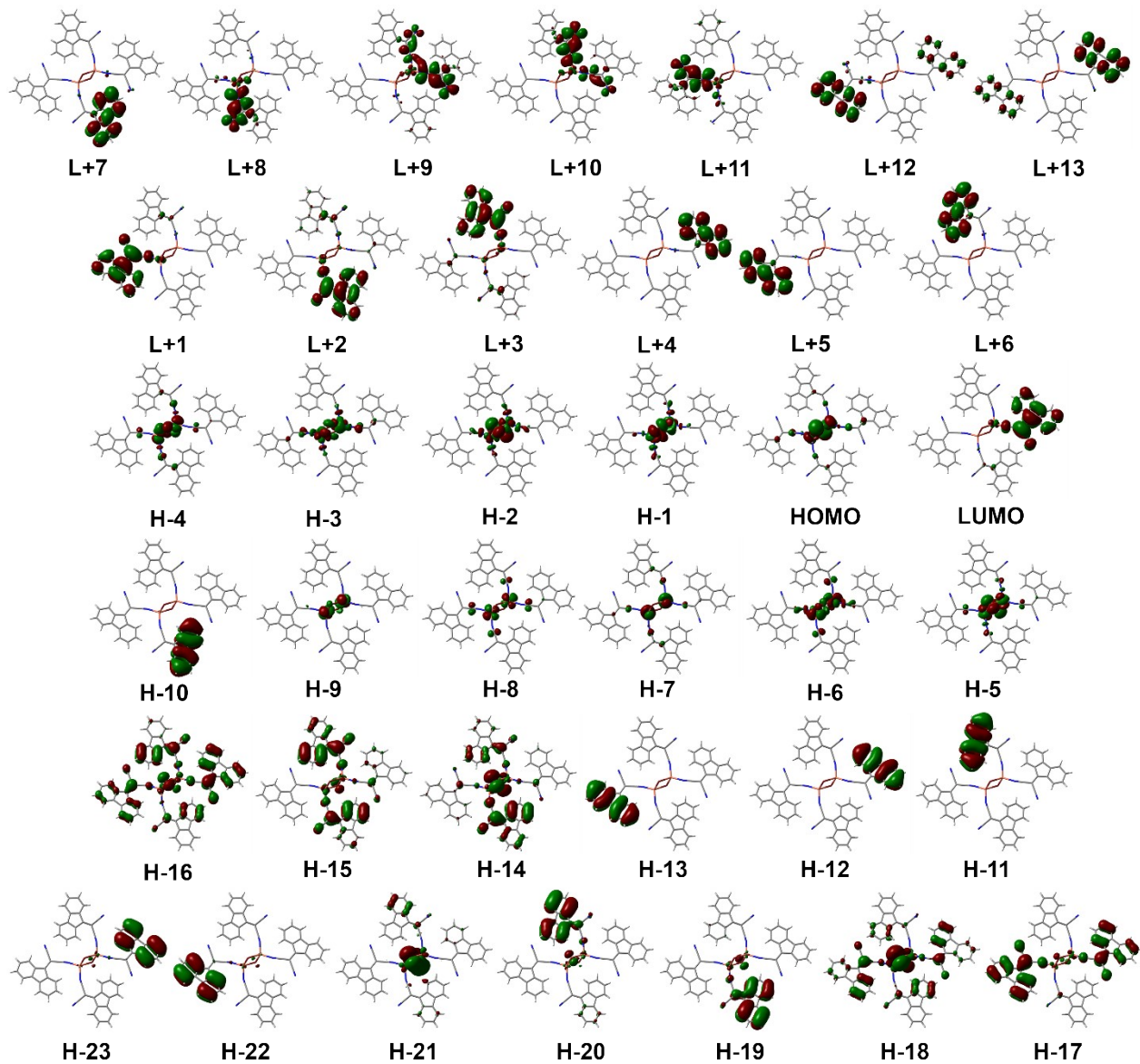


Figure S15. Selected molecular orbitals of the  $\text{Cu}_2\text{Br}_2\text{L}_4$  cluster.

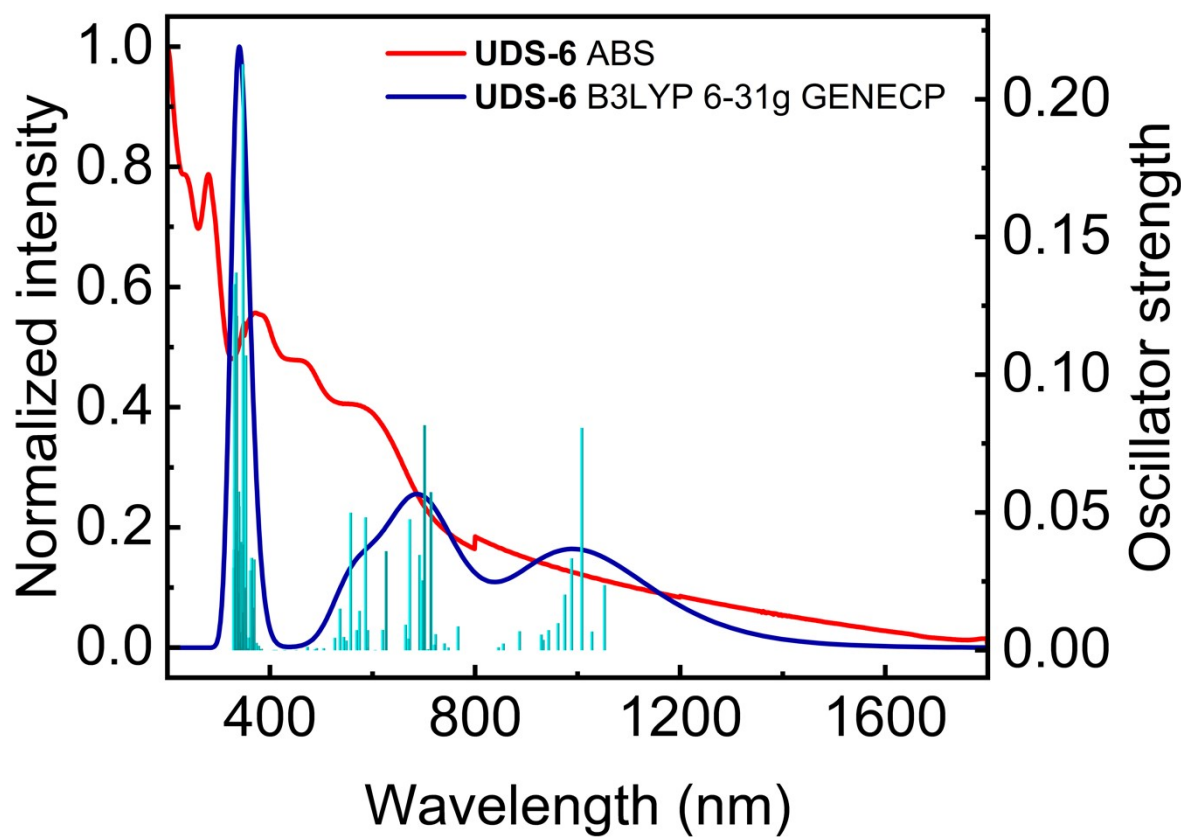


Figure S16. Calculated UV-Vis spectrum (in blue) of **UDS-6** compared to the experimental spectrum (in red). The thin cyan bars represent the individual transitions, to which a FWHM was attributed to compute the spectrum.

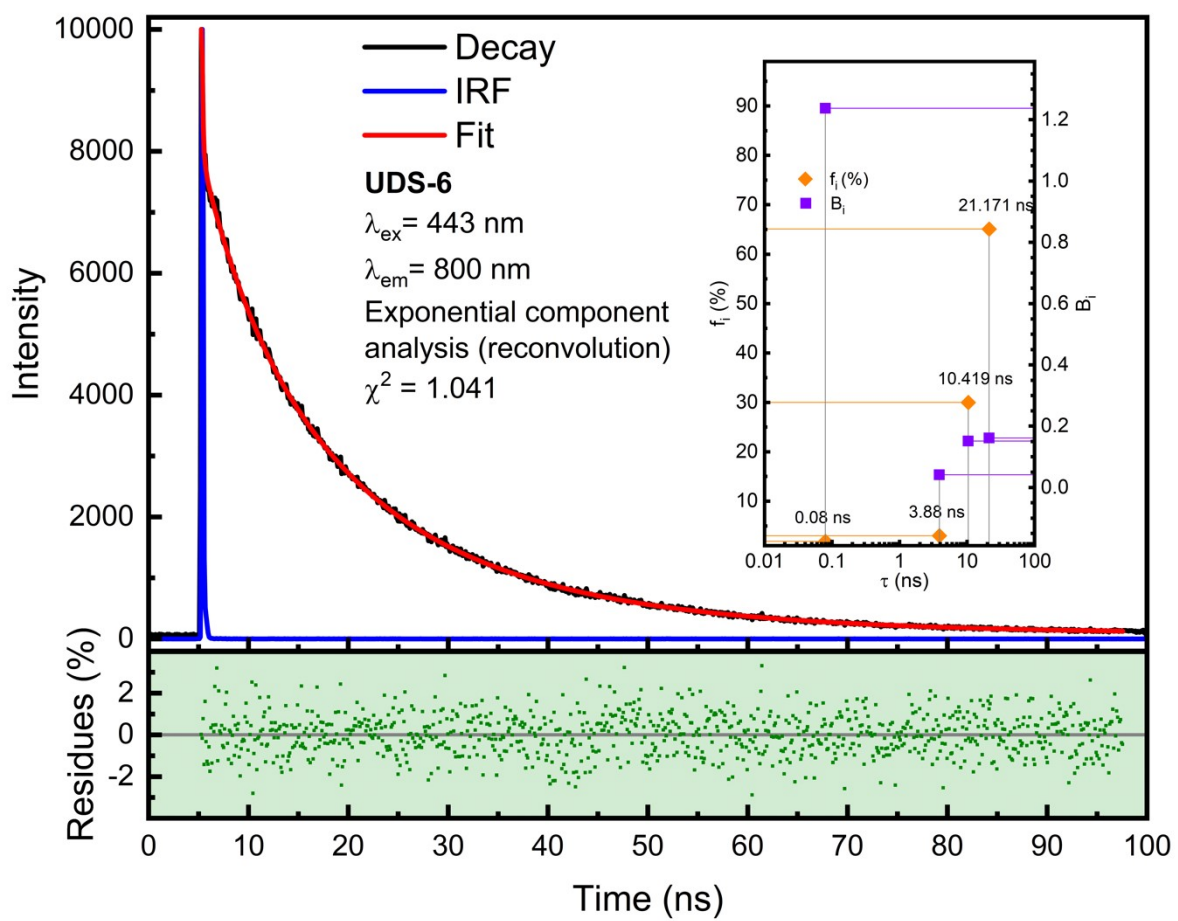


Figure S17. Photoluminescence decay of **UDS-6** at room temperature.

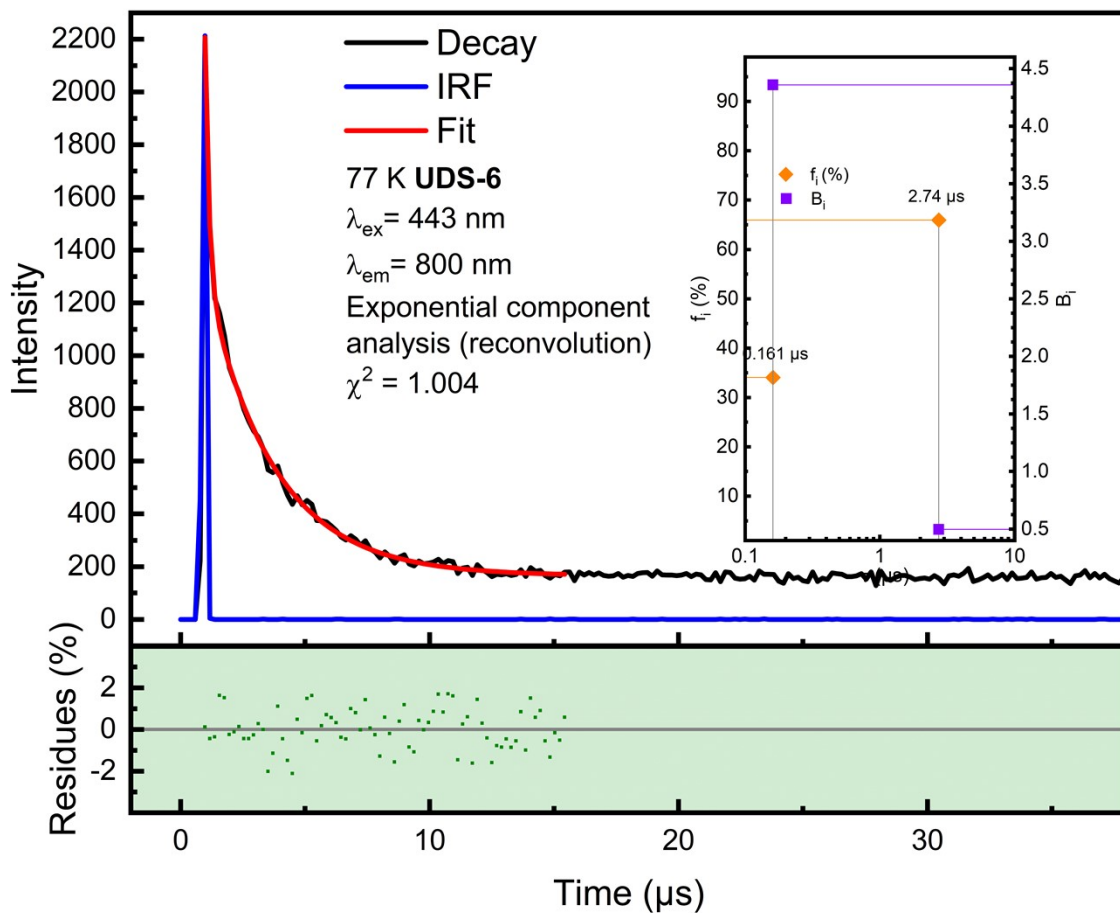


Figure S18. Photoluminescence decay and lifetime of UDS-6 at 77K. A low intensity forced the use of fewer channels. A long component ( $\mu\text{s}$ ) can be observed by the long tailing.

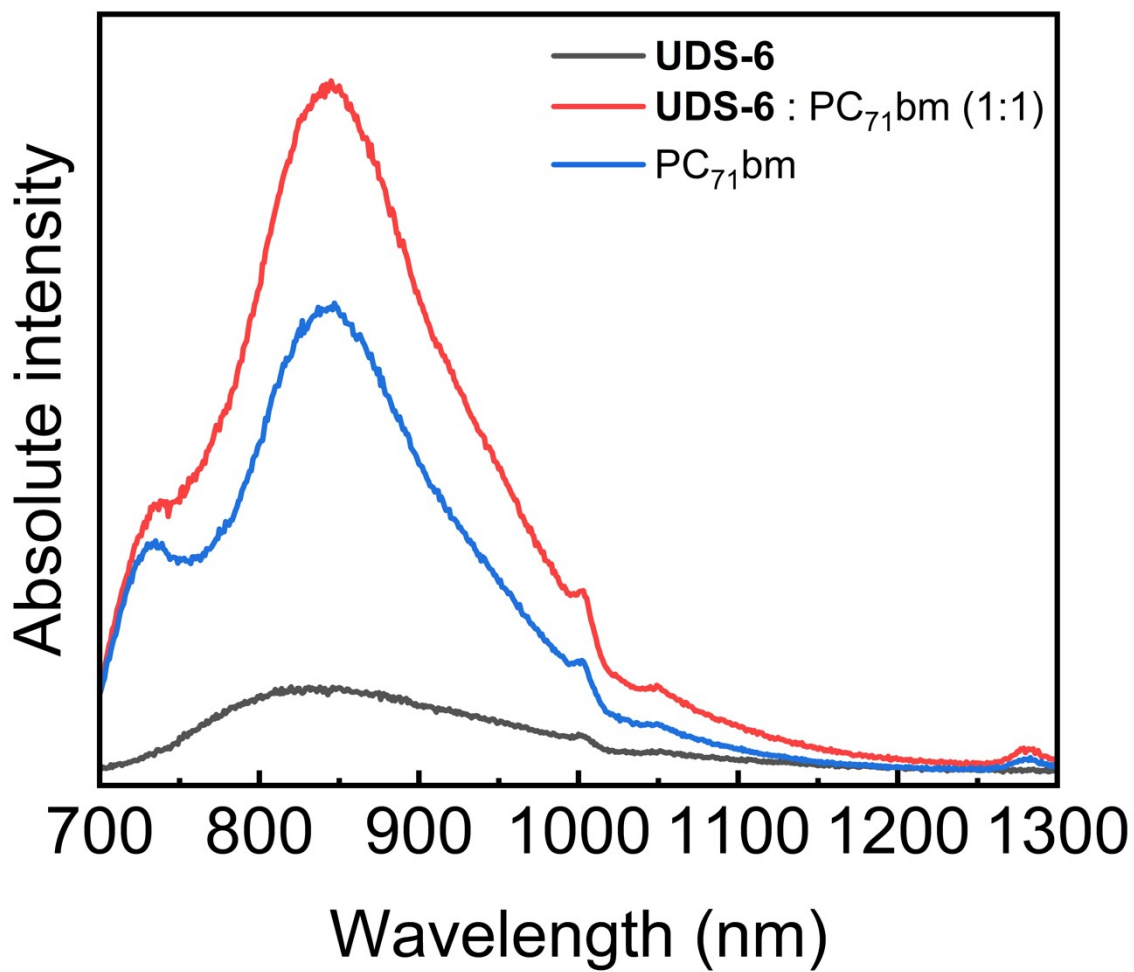


Figure S19. Photoluminescence spectra of different powders. There is no significant interaction between **UDS-6** and PC<sub>71</sub>bm, as the luminescence of PC71bm is not reduced by at least half of the initial intensity.

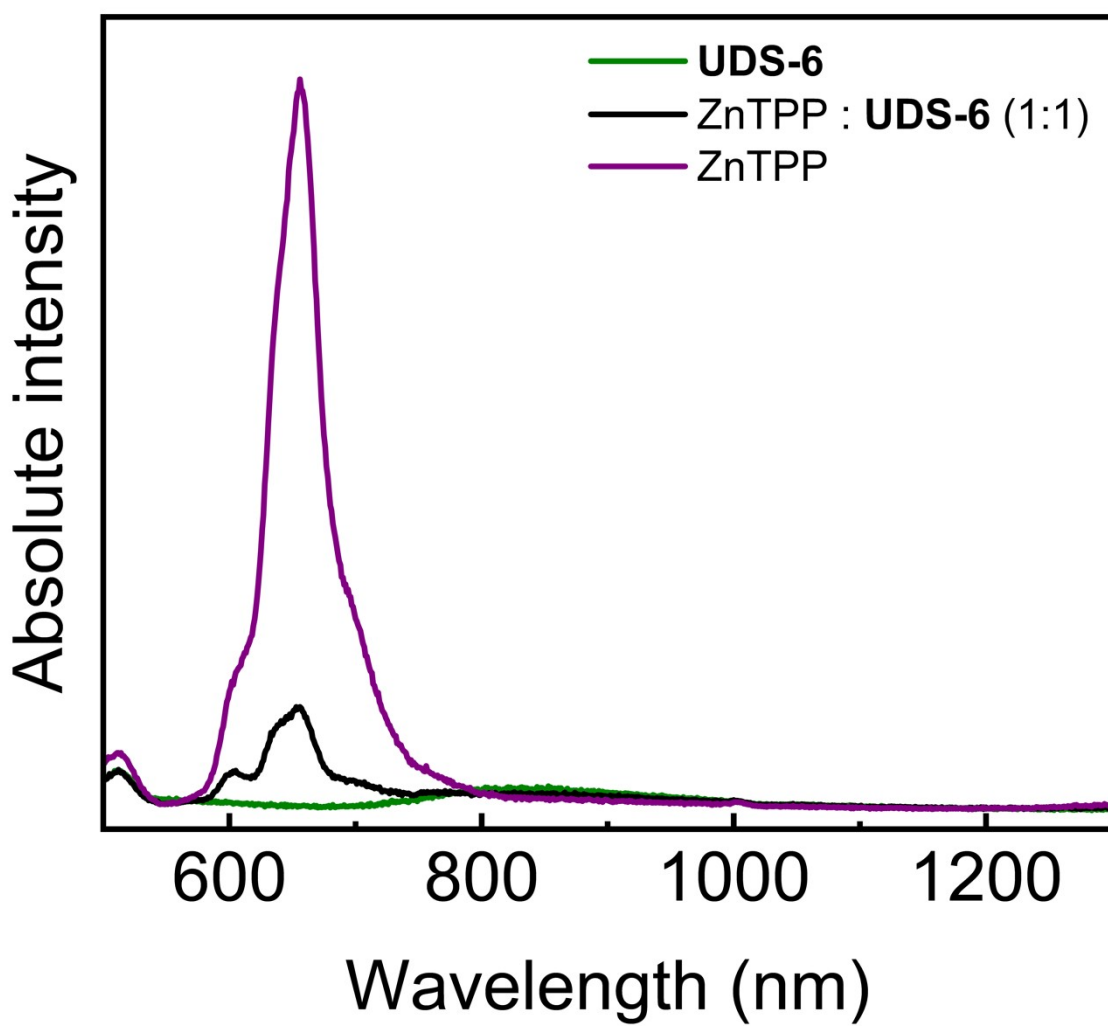


Figure S20. Photoluminescence quenching of ZnTPP by **UDS-6** seen by the decrease in the PL of both chromophores. The remaining PL intensity in ZnTPP suggests a not completely efficient quenching mechanism.

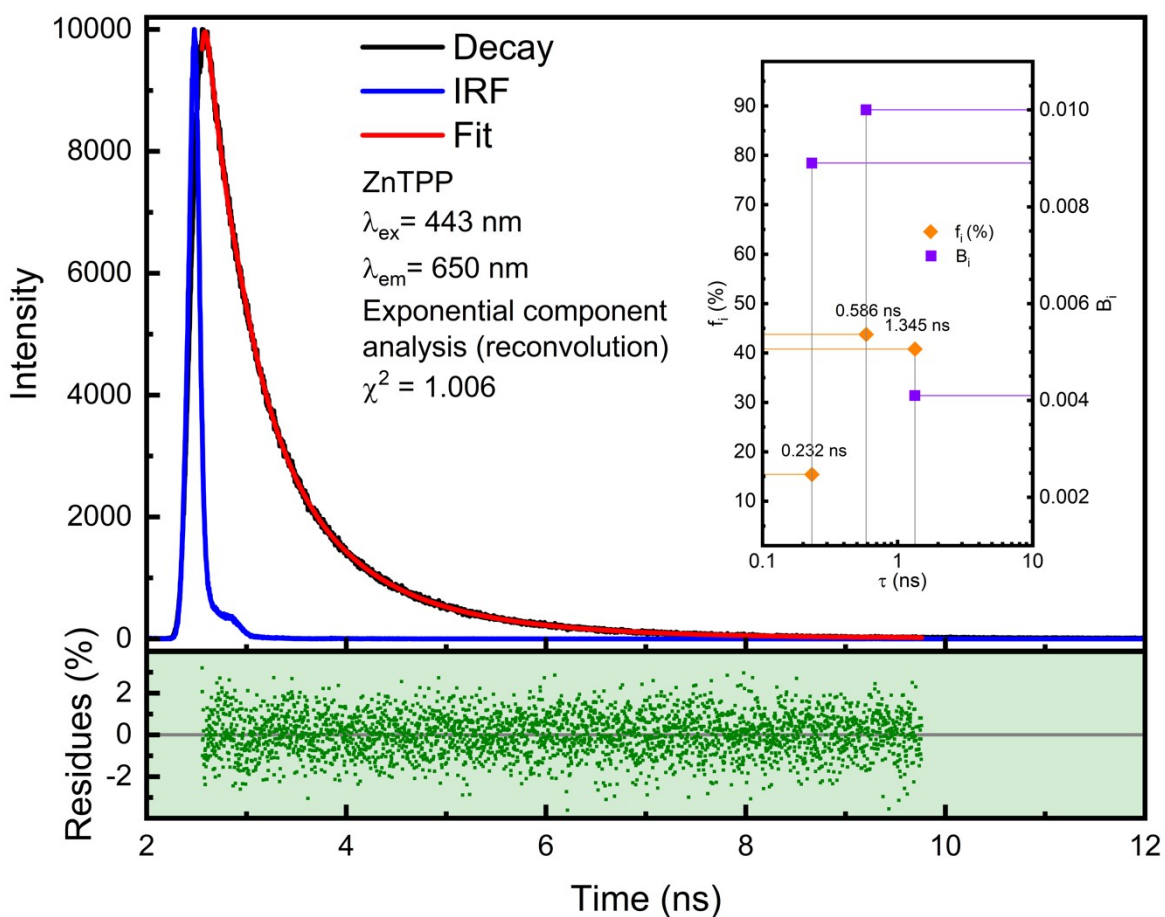


Figure S21. Photoluminescence decay and lifetimes of ZnTPP in the solid state.

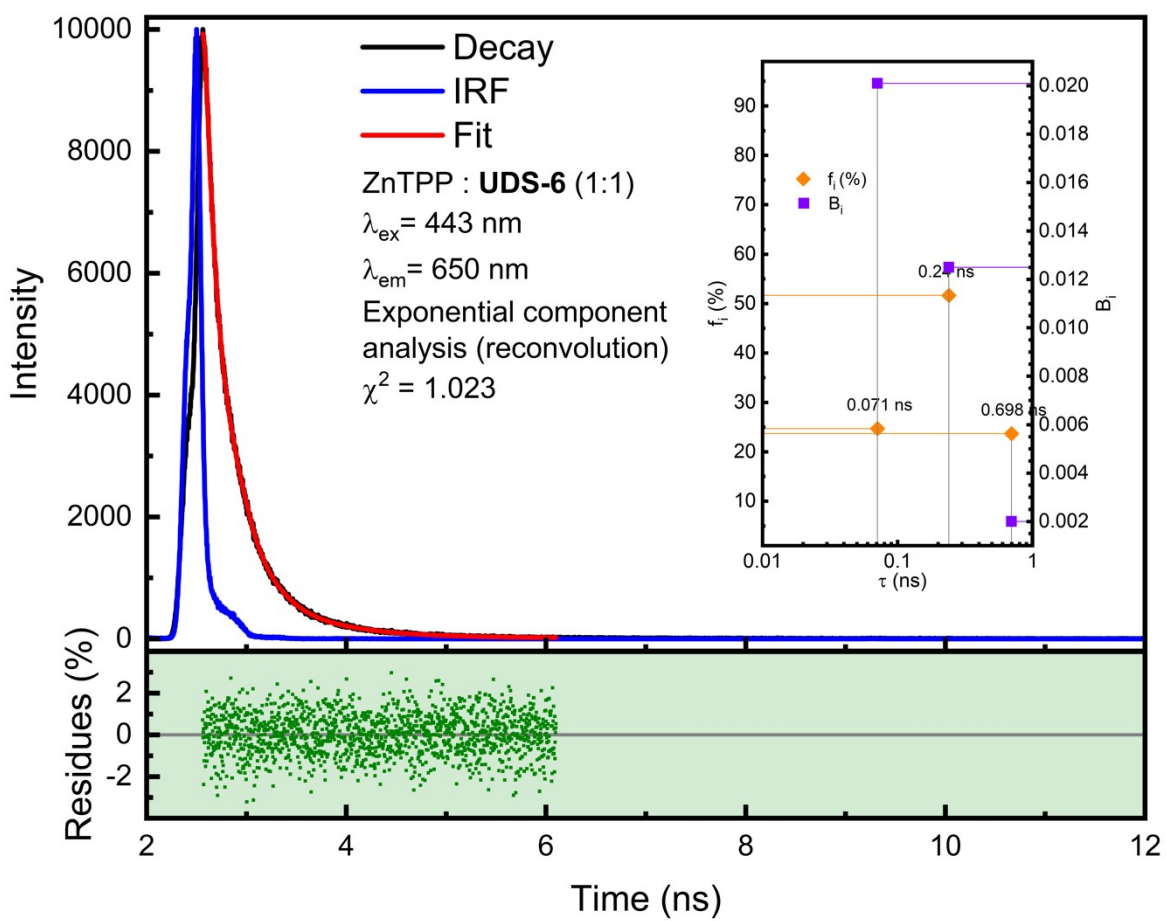


Figure S22. Photoluminescence decay and lifetimes of ZnTPP in a solid state blend with **UDS-6**.

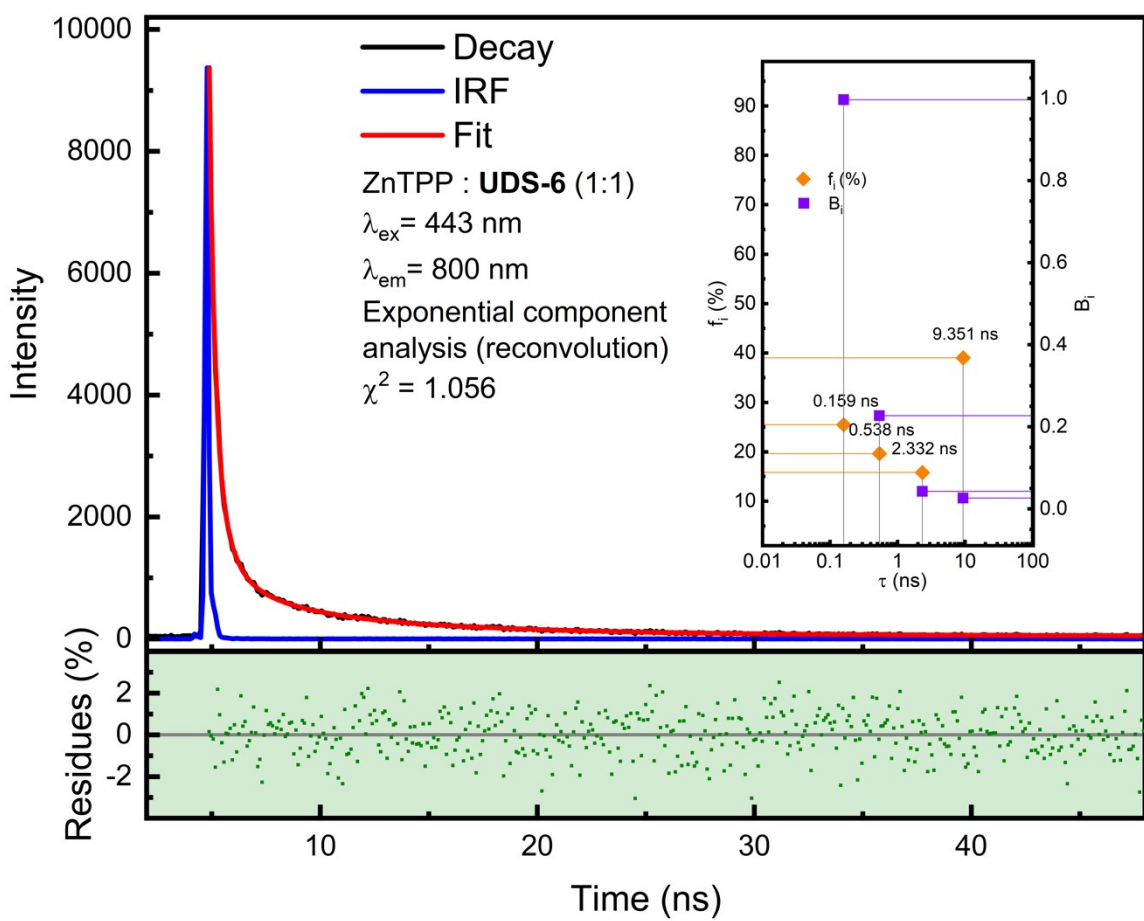


Figure S23. Photoluminescence decay and lifetimes of **UDS-6** in a blend with ZnTPP.

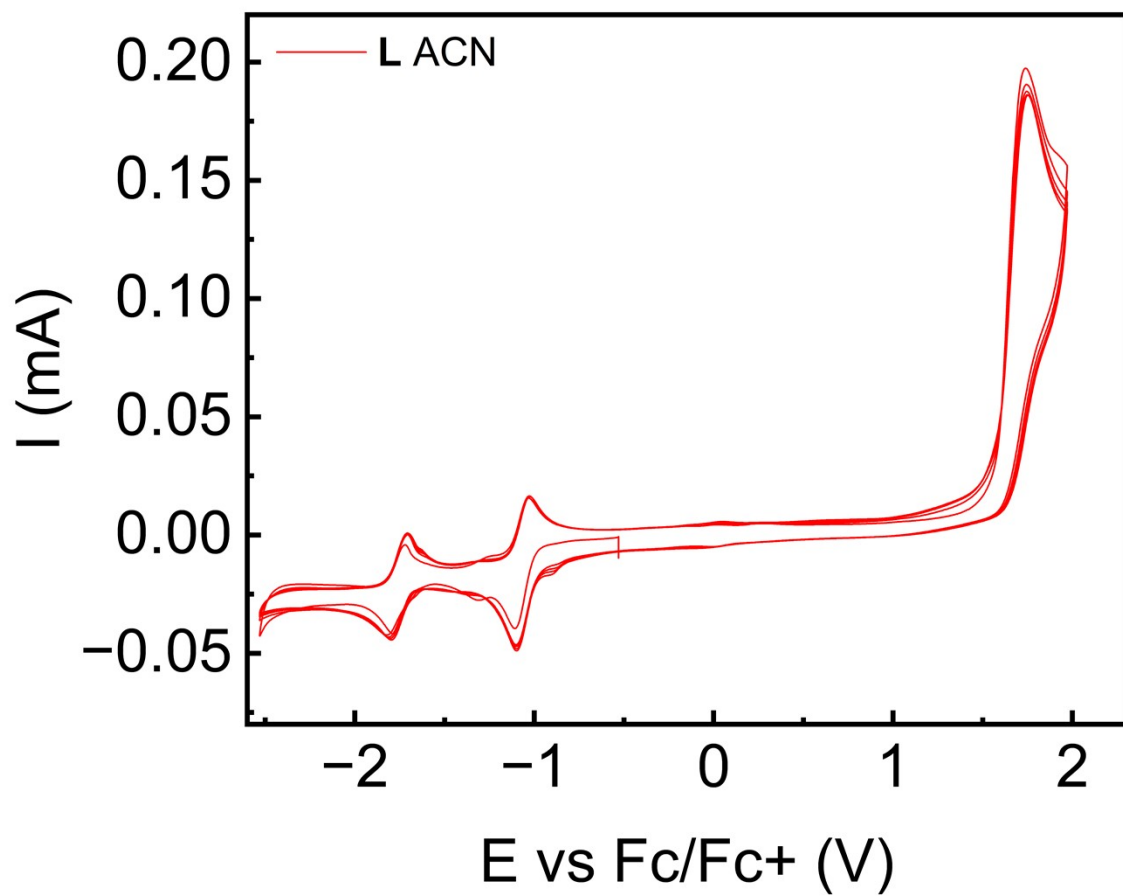


Figure S24. Cyclic voltammetry plot of **L** in dry degassed ACN.

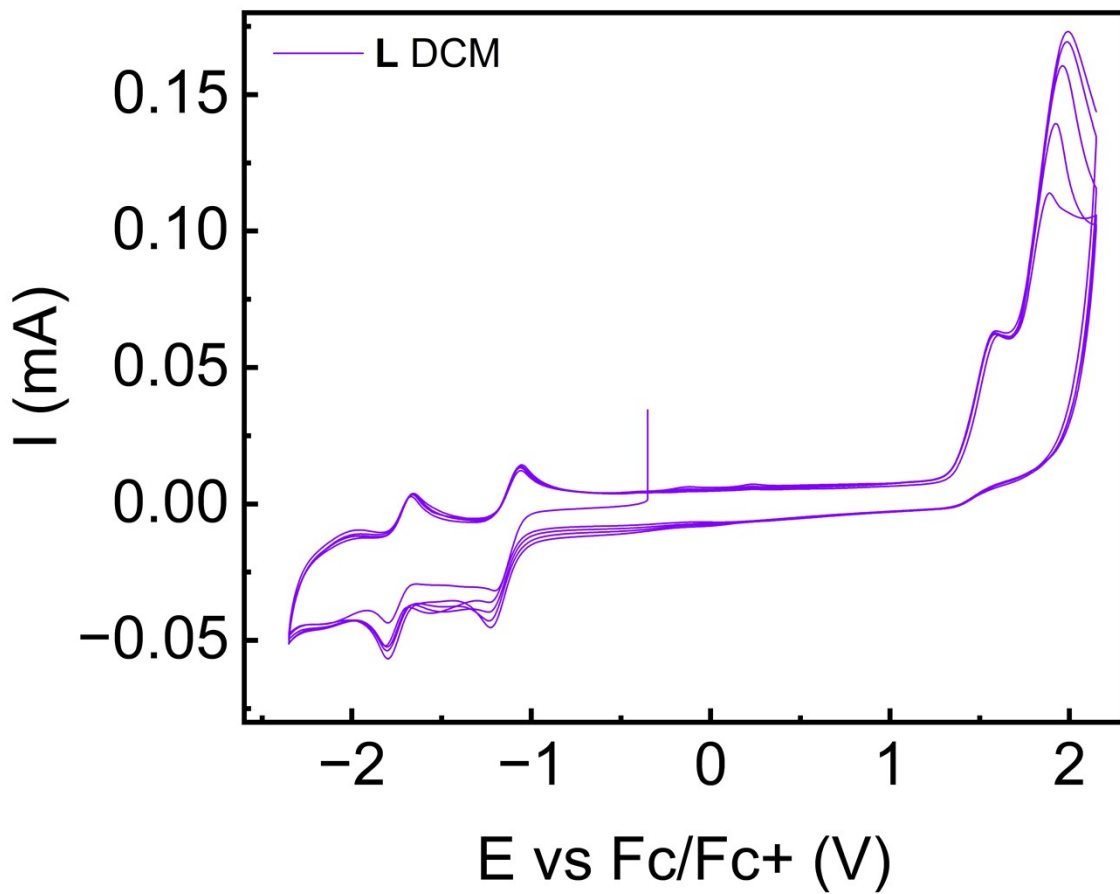


Figure S25. Cyclic voltammetry plot of **L** in dry degassed DCM.

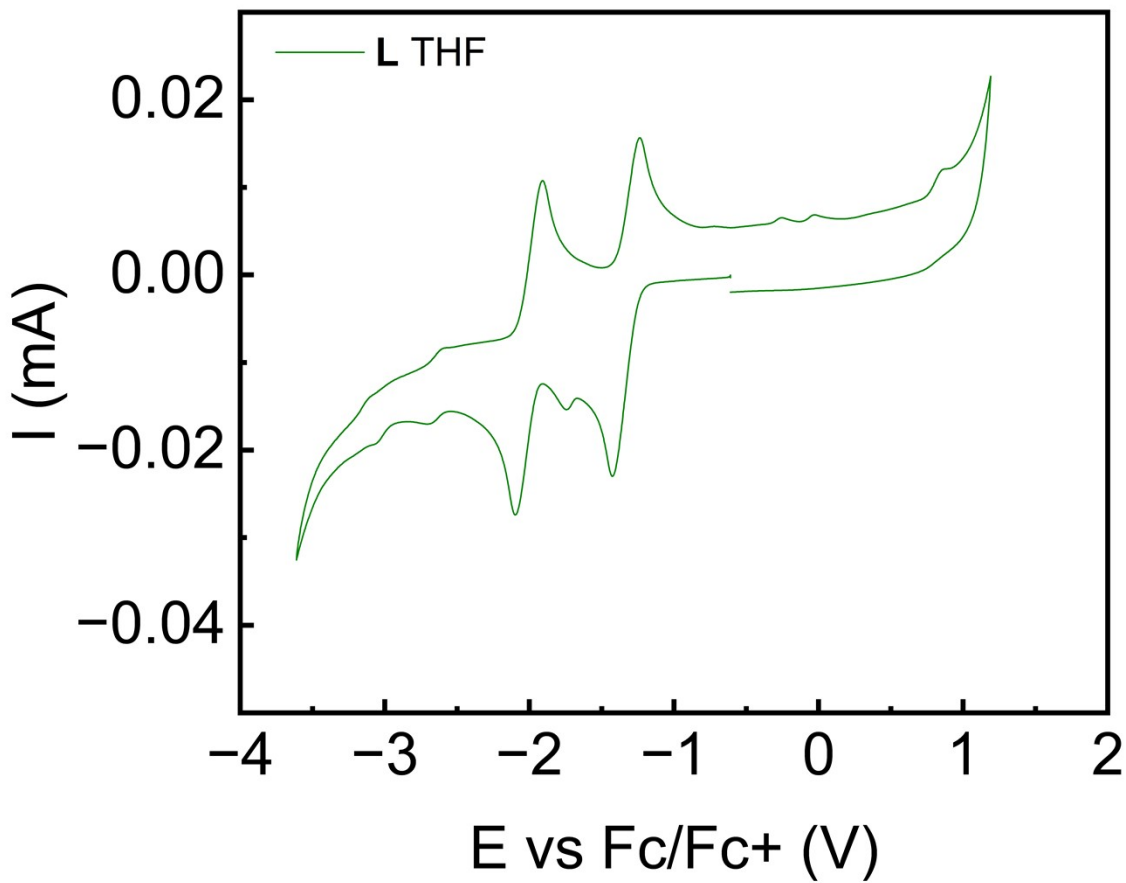


Figure S26. Cyclic voltammetry plot of **L** in dry degassed THF. Since **L** precipitates on the electrode after the first cycle, only this first cycle is presented here.

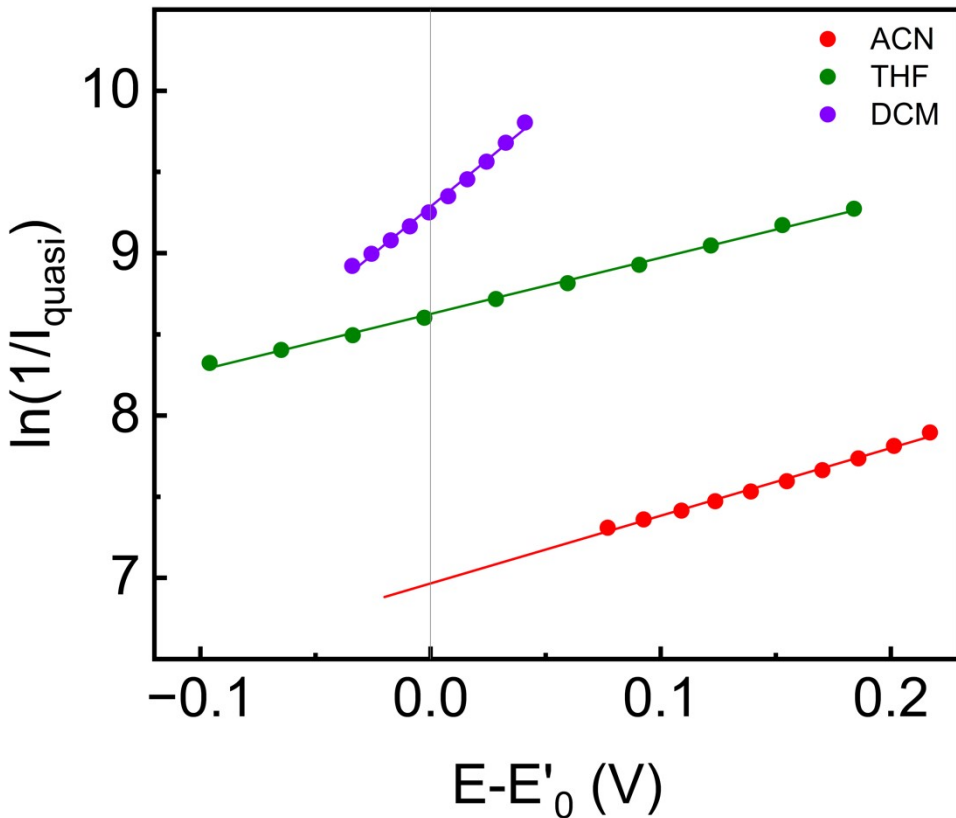


Figure S27. Kinetic parameter determination for **L** using rotating disk electrodes adapted for a quasi-reversible system. The  $I_{\text{quasi}}$  was obtained from Koutecký-Levich plot from the intercept at different overpotential with acetonitrile, tetrahydrofuran and dichloromethane. The heterogenous standard rate constant was estimated using linear regression and equation 1.

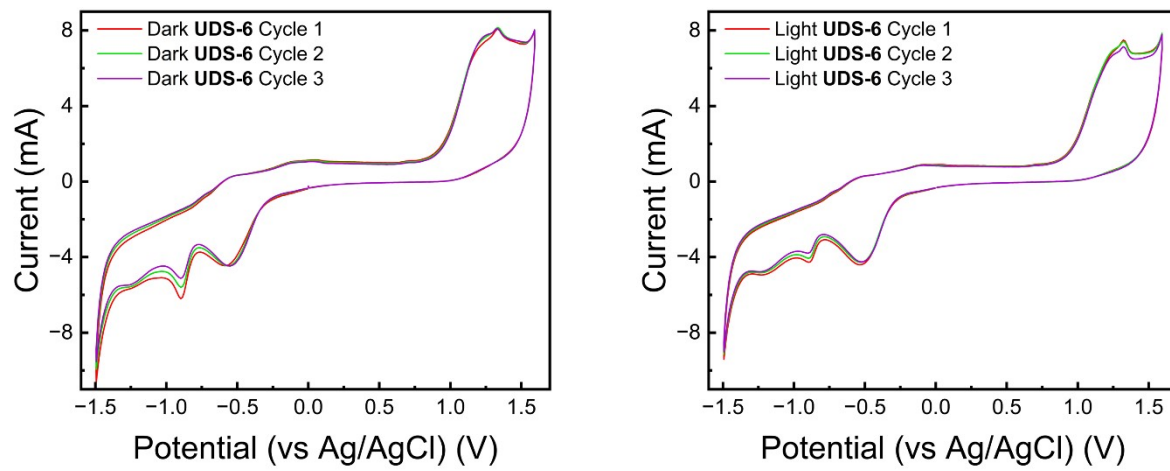


Figure S28. Cyclic voltammetry of a spin-coated dispersed film of **UDS-6** shows no difference between dark conditions (left) and simulated solar irradiance exposure (right).

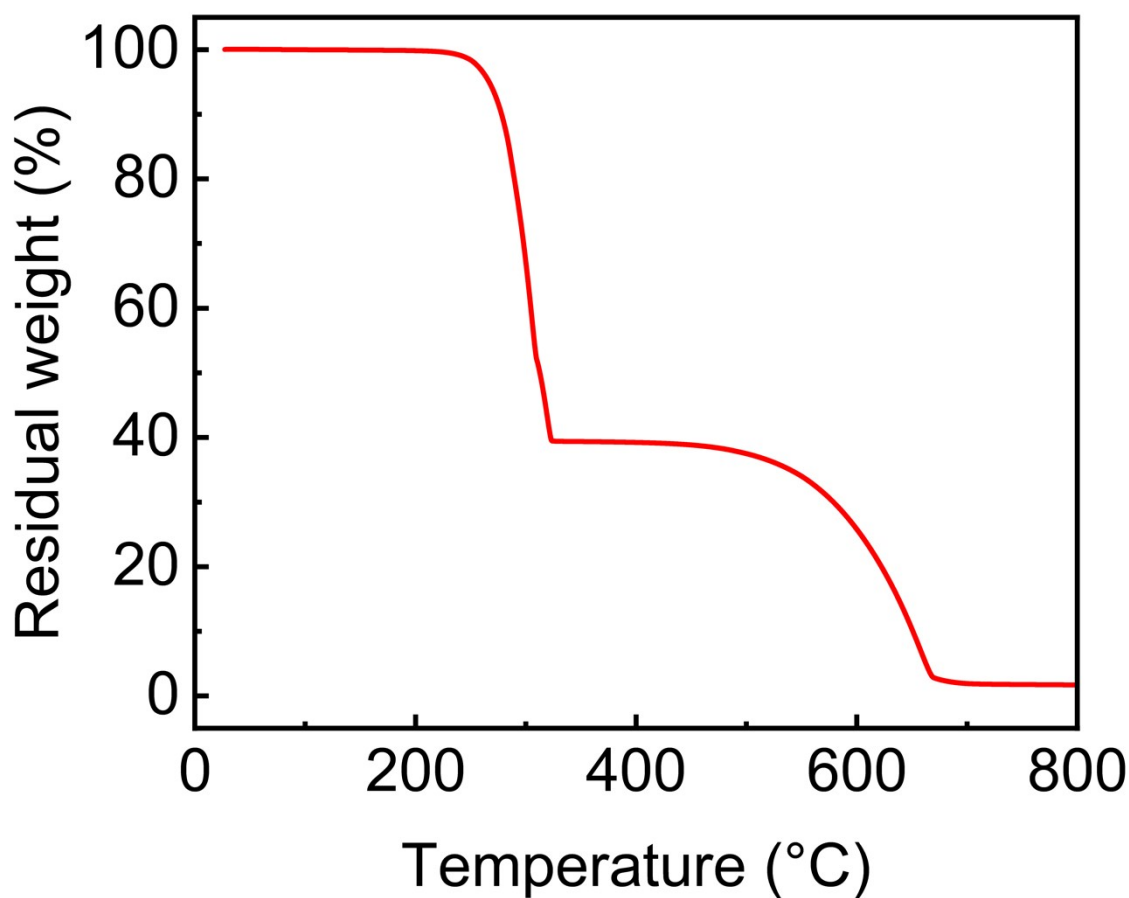


Figure S29. Thermogravimetric analysis plot of the thermal degradation of **UDS-6**.

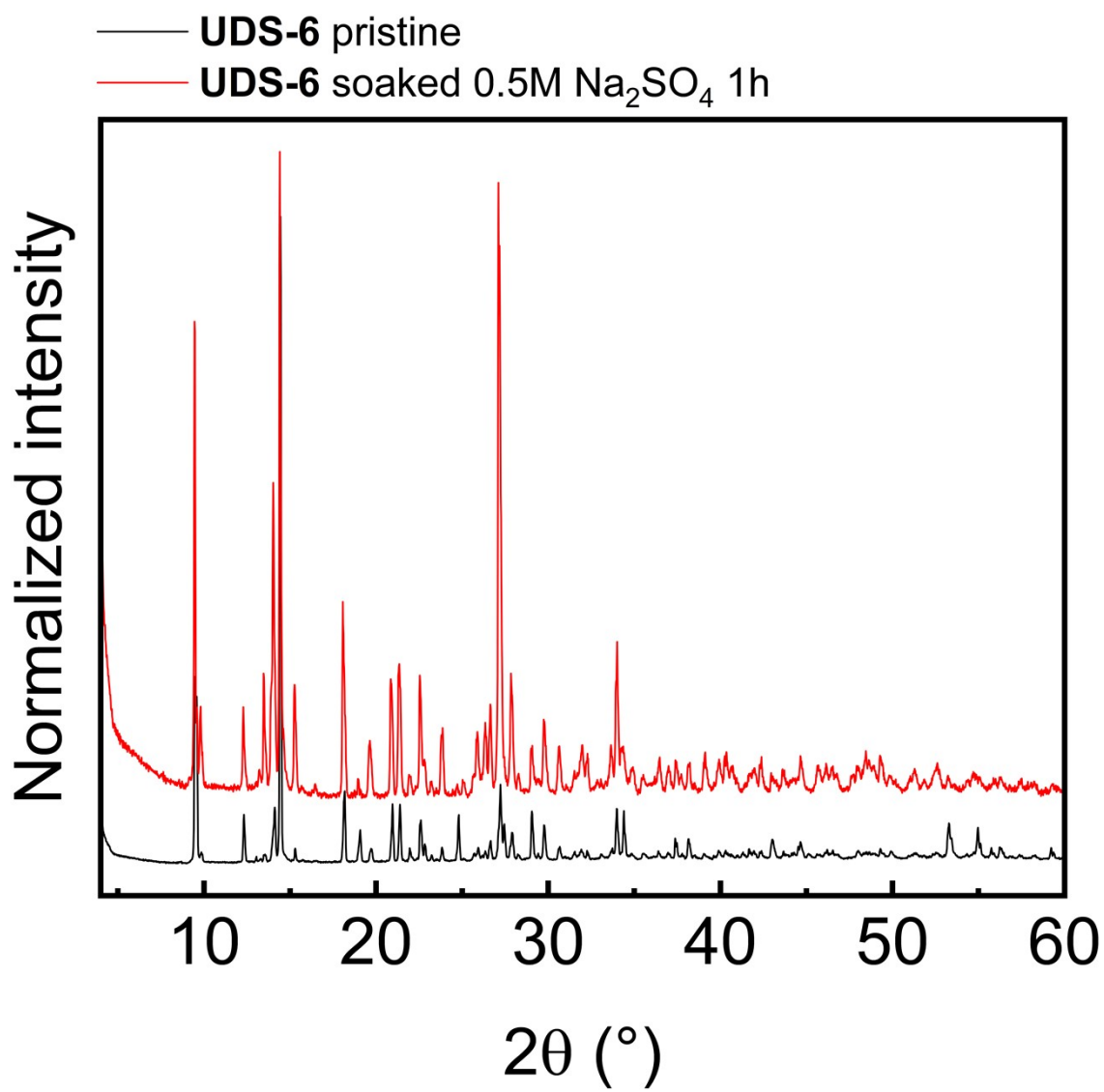


Figure S30. Powder X-ray diffractogram of a pristine sample of **UDS-6**, and a sample of **UDS-6** soaked for one hour in aqueous 0.5M Na<sub>2</sub>SO<sub>4</sub>.